nature immunology

Trans-presentation of IL-6 by dendritic cells is required for the priming of pathogenic T_H17 cells

Sylvia Heink[1,14], Nir Yogev[2,13,14], Christoph Garbers[3], Marina Herwerth[1,4], Lilian Aly[1], Christiane Gasperi[1], Veronika Husterer[1], Andrew L Croxford[2], Katja Möller-Hackbarth[3], Harald S Bartsch[5], Karl Sotlar[5], Stefan Krebs[6], Tommy Regen[2], Helmut Blum[6], Bernhard Hemmer[1,7], Thomas Misgeld[4,7], Thomas F Wunderlich[8], Juan Hidalgo[9], Mohamed Oukka[10,11], Stefan Rose-John[3], Marc Schmidt-Supprian[12], Ari Waisman[2,15] & Thomas Korn[1,7,15]

The cellular sources of interleukin 6 (IL-6) that are relevant for differentiation of the T_H17 subset of helper T cells remain unclear. Here we used a novel strategy for the conditional deletion of distinct IL-6-producing cell types to show that dendritic cells (DCs) positive for the signaling regulator Sirpα were essential for the generation of pathogenic T_H17 cells. Using their IL-6 receptor α-chain (IL-6Rα), Sirpα$^+$ DCs trans-presented IL-6 to T cells during the process of cognate interaction. While ambient IL-6 was sufficient to suppress the induction of expression of the transcription factor Foxp3 in T cells, trans-presentation of IL-6 by DC-bound IL-6Rα (called 'IL-6 cluster signaling' here) was needed to prevent premature induction of interferon-γ (IFN-γ) expression in T cells and to generate pathogenic T_H17 cells *in vivo*. Our findings should guide therapeutic approaches for the treatment of T_H17-cell-mediated autoimmune diseases.

During antigen-specific priming, CD4$^+$ helper T cells differentiate into distinct subsets characterized by specific master transcription factors and signature cytokines. The differentiation process is controlled by various cytokines present in the micro-environment, in which CD4$^+$ T cells interact in a cognate way with antigen-presenting cells (APCs). Because stimulation of the T cell antigen receptor (TCR) in the presence of the ubiquitously expressed cytokine TGF-β results in the induction of expression of the transcription factor Foxp3, productive effector T cell responses require efficient ways to suppress such induction in T cells during priming. Although interleukin 27 (IL-27) has additional regulatory functions[1], IL-27 and IL-4 are strong inhibitors of the induction of Foxp3 expression during the development of T_H1 cells and T_H2 cells, respectively[2–4]. During T_H17 cell development, IL-6 prevents transcription of the gene encoding Foxp3 and at the same time induces IL-17 (refs. 5,6). However, it is unclear whether these functions of IL-6 are connected with each other or are independent events.

T_H17 cells are categorized as pathogenic or non-pathogenic depending on whether or not they have sensed IL-23 (refs. 7,8). However, single-cell analysis of T_H17 cells isolated from the inflamed central nervous system (CNS) has revealed that individual T_H17 cells can exhibit a non-pathogenic gene signature, including the expression of genes encoding transcription factors (*Eomes*, *Irf8* and *Maf*), cytokines (*Il24* and *Il9*) and surface receptors (*Cxcr6* and *Cd96*), although they express the cytokine-receptor-encoding gene *Il23r*[9]. Thus, the 'decision' of whether a T_H17 cell will become pathogenic can be taken independently of IL-23 and might be made early during priming.

Because IL-6 is the dominant factor that initiates the transcriptional program of T_H17 cells, we speculated that intrinsic properties of IL-6 might be a major determinant of the priming of pathogenic T cells. To signal into target cells, IL-6 first binds to its receptor subunit IL-6Rα. That complex then associates with gp130 (the signaling subunit of the IL-6 receptor), which results in a heterohexameric signaling complex (IL-6, IL-6Rα and gp130 in a stoichiometry of 2:2:2) that triggers productive signaling via IL-6 into the target cell[10,11]. In addition to its membrane form, IL-6Rα can be shed and bind IL-6 as a soluble receptor. The soluble complex of IL-6 and soluble IL-6Rα (sIL-6Rα) associates with gp130 and initiates IL-6 signaling in gp130$^+$ cells. This type of IL-6 signaling is called 'IL-6 trans-signaling'[12,13]. In contrast to classic IL-6 signaling, IL-6 trans-signaling can be blocked by soluble gp130, which acts as a decoy receptor for the soluble IL-6–IL-6Rα complex[14].

Here, to investigate whether the cellular source of IL-6 was a determinant of T_H17 cell fate, we developed a novel IL-6-reporter strategy

[1]Klinikum rechts der Isar, Department of Neurology, Technical University of Munich, Munich, Germany. [2]Institute for Molecular Medicine, University Medical Center of the Johannes Gutenberg University, Mainz, Germany. [3]Institute of Biochemistry, Kiel University, Kiel, Germany. [4]Institute of Neuronal Cell Biology, Technical University of Munich, Munich, Germany. [5]Institute of Pathology, Medical School, Ludwig-Maximilians-University, Munich, Germany. [6]Gene Centre, Lafuga, Ludwig-Maximilians-University, Munich, Germany. [7]Munich Cluster for Systems Neurology (SyNergy), Munich, Germany. [8]Max Planck Institute for Metabolism Research, Cologne, Germany. [9]Department of Cellular Biology, Physiology, and Immunology, Autonomous University of Barcelona, Barcelona, Spain. [10]Department of Immunology, University of Washington, Seattle, Washington, USA. [11]Center for Immunity and Immunotherapies, Seattle Children's Research Institute, Seattle, Washington, USA. [12]Department of Hematology and Oncology, Klinikum rechts der Isar, Technical University of Munich, Munich, Germany. [13]Present address: Department of Neurology, University Medical Center of the Johannes Gutenberg University, Mainz, Germany. [14]These authors contributed equally to this work. [15]These authors jointly directed this work. Correspondence should be addressed to T.K. (thomas.korn@tum.de).

Received 9 May; accepted 4 November; published online 28 November 2016; corrected after print 23 January 2017; doi:10.1038/ni.3632

that allowed the deletion of IL-6-expressing subsets within distinct cell populations. We found that a subset of CD11b$^+$ DCs that were Sirpα^+ were indispensable for the priming of myelin-peptide-specific encephalitogenic T cells. Our data indicated that CD11b$^+$Sirpα^+ DCs were able to trans-present IL-6 through a complex containing DC-expressed IL-6Rα bound to IL-6 that was able to interact with gp130 expressed on T cells. We define this mode of IL-6 signaling as 'cluster signaling' and propose that the 'imprinting' of encephalitogenic properties on effector T cells is dependent on IL-6 cluster signaling, while classic signaling by IL-6 through its membrane-bound receptor complex is sufficient to suppress the TGF-β-induced expression of Foxp3 but fails to prime pathogenic T_H17 cells.

RESULTS

DC-derived IL-6 is indispensable for pathogenic T_H17 cells

Because IL-6 is produced by various hematopoietic and non-hematopoietic cells, we sought to define the relevant cellular source of IL-6 for the differentiation of pathogenic T_H17 cells. We generated an IL-6-reporter knock-in allele (*Il6*RD) in which IL-6 expression is reported by expression of the cyan fluorescent protein Cerulean and alloantigen Thy1.1 (**Supplementary Fig. 1**). In addition, the reporter contains a *lox*P-flanked stop cassette (*Stop*$^{flox/flox}$) that allows cell-type-specific expression of the reporter cassette depending on the driver of Cre recombinase expression used in various mouse strains. First we crossed *Il6*$^{RD/wt}$ mice with a CMV-Cre deleter strain to allow unrestricted expression of the IL-6-reporter cassette, then we immunized the progeny of that cross with the peptide MOG(35–55) in complete Freund's adjuvant (CFA) to induce experimental autoimmune encephalomyelitis (EAE). On day 7 after immunization, Thy1.1 (IL-6) was produced exclusively by CD45$^+$ hematopoietic cells in draining lymph node cells and spleen of CMV-Cre × *Il6*$^{RD/wt}$ mice (**Fig. 1a**). CD11c$^+$ cell populations had the greatest frequency of Thy1.1$^+$ (IL-6$^+$) cells (**Fig. 1a**). Subgroup analysis revealed that expression of Thy1.1 (IL-6) was restricted to CD11b$^+$Sirpα^+CD103$^-$SiglecH$^-$ DCs (**Supplementary Fig. 2**). We used CD11c-Cre × *Il6*$^{RD/wt}$ × R26 *Stop*$^{flox/flox}$ YFP mice (which express yellow fluorescent protein (YFP) under control of the *Rosa26* (R26) promoter after Cre-mediated deletion of the *Stop*$^{flox/flox}$ cassette to simultaneously monitor DCs (via YFP expression (under control of the R26 promoter) in CD11c$^+$ cells)) and IL-6 production in DCs (via Thy1.1 expression (under control of the endogenous *Il6* promoter) in CD11c$^+$ cells). We noticed that some DCs in the draining lymph nodes of these mice were Thy1.1$^+$ as early as the first day after immunization with MOG(35–55) in CFA (**Fig. 1b**). That subset of Thy1.1$^+$ DCs was maintained at least through day 6 after immunization (**Fig. 1b**). At the peak of EAE (day 16 after immunization), Thy1.1$^+$ cells in the CNS of CMV-Cre × *Il6*$^{RD/wt}$ mice were mainly CD45$^+$CD11b$^+$ myeloid cells (**Fig. 1c**). Nevertheless, and in contrast to results obtained for the peripheral immune compartment, a substantial portion of IL-6 in the CNS seemed to be produced by non-hematopoietic (CD45$^-$) cells (**Fig. 1c**). Notably, specific ablation of IL-6-producing DCs in CD11c-Cre × *Il6*$^{RD/wt}$ mice through the use of antibody to Thy1.1 (anti-Thy1.1) (**Supplementary Fig. 2**) resulted in the priming of MOG(35–55)-specific T cells with reduced expression of IL-17 and increased expression of IFN-γ relative to that of the cytokine expression of MOG(35–55)-specific T cells isolated from CD11c-Cre × *Il6*$^{RD/wt}$ mice treated with control antibody (**Fig. 1d** and **Supplementary Fig. 3**). Moreover, treatment of CD11c-Cre × *Il6*$^{RD/wt}$ mice with anti-Thy1.1 abrogated their development of EAE (**Fig. 1e**). These data suggested that either IL-6 production by DCs or the physical presence of IL-6-producing DCs was required for the induction of EAE. To distinguish between those possibilities, we conditionally deleted *Il6* in DCs through the use of mice expressing CD11c-Cre and *lox*P-flanked *Il6* alleles (*Il6*$^{flox/flox}$). The loss of *Il6* in DCs in CD11c-Cre × *Il6*$^{flox/flox}$ mice (called '*Il6*^{ΔDC}' here) resulted in complete resistance to EAE, despite the continued presence of CD11b$^+$Sirpα^+ DCs in these mice (**Fig. 1f**). Indeed, *Il6*^{ΔDC} mice were a phenocopy of *Il6*$^{-/-}$ mice in their resistance to EAE (data not shown). Apart from its expression by DCs, some Thy1.1 (IL-6) was expressed by T cells, B cells and macrophages (**Fig. 1a**). Conditional deletion of *Il6* in these cells modulated disease severity but did not abrogate the development of EAE (**Supplementary Fig. 4**). Thus, DC-derived IL-6 was essential for the priming of a pathogenic T cell response in EAE.

Specific sensing of DC-derived IL-6 by interacting T cells

Our data would be consistent with the idea that DC-derived IL-6 'acted back' on DCs in an autocrine manner to boost their ability to prime pathogenic T_H17 cells. However, we found no major differences between *Il6ra*$^{flox/flox}$ (control) bone-marrow-derived DCs (BMDCs) and IL-6Rα-deficient BMDCs (derived from CD11c-Cre × *Il6ra*$^{flox/flox}$ (*Il6ra*^{ΔDC}) mice, which cannot respond to soluble IL-6) in their induction of *Il1b*, *Il12* or *Il23* after exposure to exogenous IL-6 (**Supplementary Fig. 5**). Thus, we explored alternative modes of action for DC-derived IL-6 during cognate interaction with T cells. We obtained naive (Foxp3$^-$) CD4$^+$ T cells from 2D2 × *Foxp3gfp*.KI mice (which have transgenic expression of a MOG(35–55)-specific TCR (2D2) and in which Foxp3 expression is reported by green fluorescent protein (GFP) (*Foxp3gfp*.KI)), transferred the cells into *Il6*$^{flox/flox}$ (control) mice, *Il6*$^{-/-}$ mice or *Il6*^{ΔDC} mice, and then immunized the host mice subcutaneously with MOG(35–55) in CFA. As previously reported[15], priming of transgenic T cells in an IL-6-deficient environment in the *Il6*$^{-/-}$ mice resulted in the conversion of about 20% of the 2D2 T cells into GFP$^+$ (Foxp3$^+$) regulatory T cells (T_{reg} cells) (**Fig. 2a**). In contrast, we did not observe conversion of GFP$^-$ 2D2 T cells into GFP$^+$ 2D2 T cells during the priming of naive 2D2 T cells in the *Il6*^{ΔDC} mice (**Fig. 2a**), which indicated that IL-6 from sources other than DCs was sufficient to suppress the conversion of conventional T cells into Foxp3$^+$ T_{reg} cells during antigen-specific priming. Indeed, the systemic IL-6 measured in the serum after subcutaneous immunization with MOG(35–55) in CFA was similar in *Il6*$^{flox/flox}$ (control) mice and *Il6*^{ΔDC} mice (**Supplementary Fig. 6**).

Although the emergence of Foxp3$^+$ T_{reg} cells was suppressed equally in *Il6*^{ΔDC} mice and IL-6-sufficient (*Il6*$^{flox/flox}$) mice, *Il6*$^{flox/flox}$ mice developed EAE following immunization with MOG(35–55) in CFA, while *Il6*^{ΔDC} mice did not (**Fig. 1f**). Thus, to search for effector T cell–intrinsic features that would explain the inability of T cells primed in *Il6*^{ΔDC} mice to induce EAE, we performed RNA-sequencing analysis of GFP$^-$ (Foxp3$^-$) 2D2 T cells that we isolated from the draining lymph nodes of *Il6*$^{flox/flox}$, *Il6*$^{-/-}$ or *Il6*^{ΔDC} mice on day 6 after immunization with MOG(35–55) in CFA. We defined the set of genes expressed differentially in 2D2 T cells from *Il6*$^{-/-}$ mice relative to their expression in 2D2 T cells from *Il6*$^{flox/flox}$ (control) mice as 'IL-6 target genes' (**Supplementary Table 1**). The IL-6 target gene set was grouped as IL-6 target genes suppressed or upregulated in 2D2 T cells primed in *Il6*$^{-/-}$ mice relative to their expression in 2D2 T cells primed in *Il6*$^{flox/flox}$ (control) mice. By gene-set–enrichment analysis, we next identified those genes in the suppressed gene set whose expression was higher in 2D2 T cells primed in *Il6*$^{flox/flox}$ mice than in those primed in *Il6*^{ΔDC} mice and those genes in the upregulated gene set whose expression was higher in 2D2 T cells primed in *Il6*^{ΔDC} mice than in those primed in *Il6*$^{flox/flox}$ mice (**Fig. 2b** and **Supplementary Tables 2** and **3**). By Ingenuity pathway analysis, we then analyzed upstream pathways compatible with the expression of

those IL-6 target genes identified in 2D2 T cells primed in *Il6*$^{flox/flox}$ mice or *Il6*$^{\Delta DC}$ mice (**Supplementary Fig. 6**). We found that differential activation of the transcription factor STAT3 was the main predictor of the distinct gene-enrichment profile of 2D2 T cells primed in *Il6*$^{\Delta DC}$ mice relative to the profile of such cells primed in *Il6*$^{flox/flox}$ mice (**Supplementary Fig. 6**). Moreover, when we directly assessed

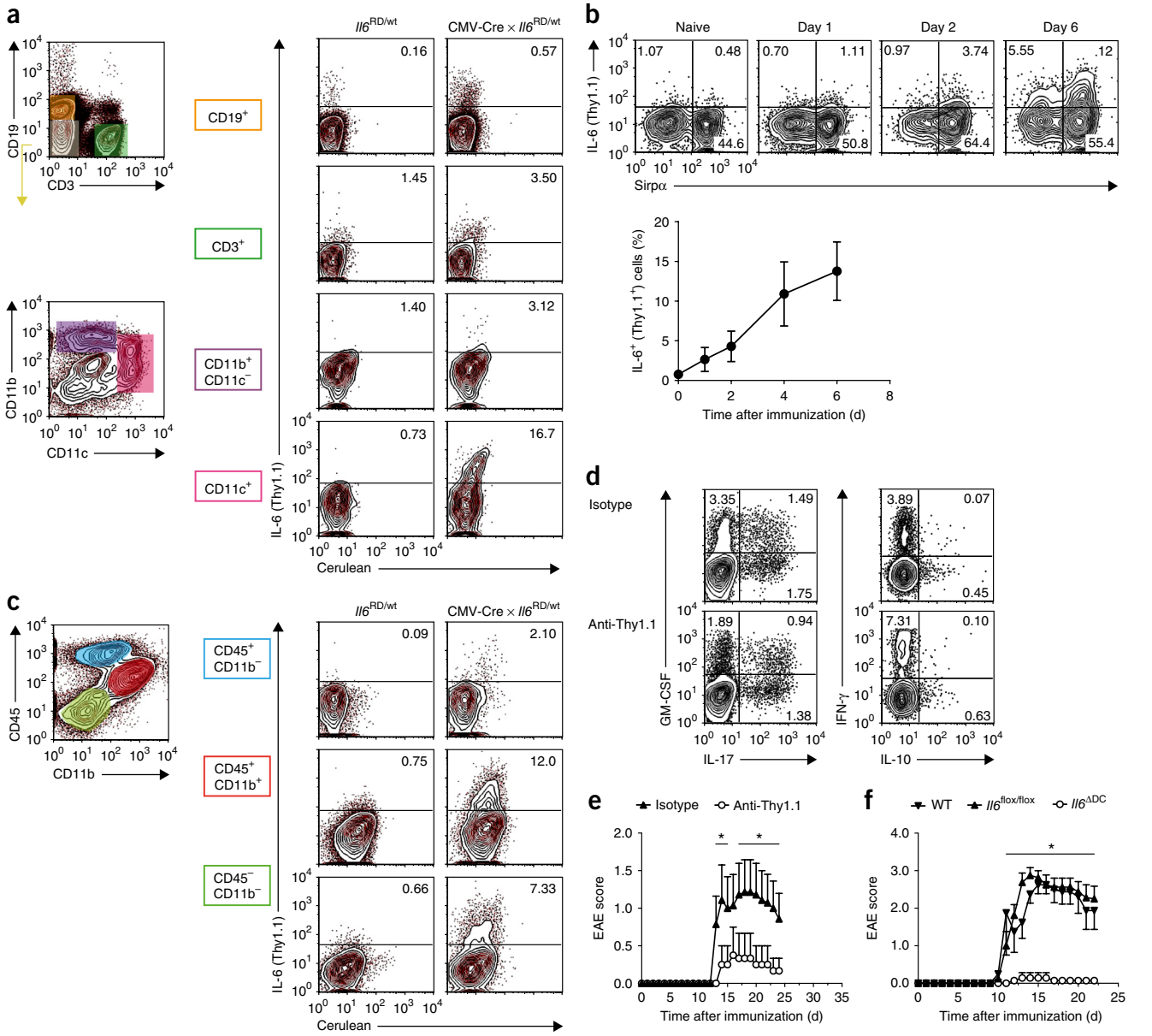

Figure 1 IL-6-producing cells during MOG(35–55)-induced EAE. (**a**) Flow cytometry of splenocytes obtained from *Il6*$^{RD/wt}$ or CMV-Cre × *Il6*$^{RD/wt}$ mice on day 7 after immunization with MOG(35–55) in CFA and stimulated for 4 h *ex vivo* with PMA and ionomycin, then gated as CD45$^+$ cells in various subsets (gating strategy (far left) shown for CMV-Cre × *Il6*$^{RD/wt}$ mice; colors of outlined areas match subsets at right), followed by analysis of the expression of IL-6 (Thy1.1) and Cerulean (middle and right) in the cell populations gated as at left (left margin). Numbers in outlined areas (middle and right) indicate percent IL-6$^+$ (Thy1.1$^+$) Cerulean$^+$ cells. (**b**) Flow cytometry analysis (top) of the expression of IL-6 (Thy1.1) and Sirpα (CD172a) by DCs (YFP$^+$CD11c$^+$MHCII^{hi}) obtained from the draining lymph nodes of CD11c-Cre × *Il6*$^{RD/wt}$ × R26 *Stop*$^{flox/flox}$ YFP mice at various times before (Naive) and after (above plots) immunization (and with *ex vivo* stimulation) as in **a**; below, kinetics of IL-6 (Thy1.1) expression in DCs as above, at various times (horizontal axis) after immunization. Numbers in quadrants (top) indicate percent cells in each (throughout). (**c**) Flow cytometry of cells obtained from the CNS of *Il6*$^{RD/wt}$ or CMV-Cre × *Il6*$^{RD/wt}$ mice on day 16 after immunization as in **a** (at the peak of EAE) and stimulated *ex vivo* as in **a**, gated as various subsets (gating strategy (far left) shown for a CMV-Cre × *Il6*$^{RD/wt}$ mouse; colors of outlined areas match subsets at right), followed by further analysis as in **a** to identify IL-6$^+$ (Thy1.1$^+$) and Cerulean$^+$ cells (middle and right). (**d**) Flow cytometry analyzing cytokine expression by CD4$^+$ T cells obtained from the draining lymph nodes of CD11c-Cre × *Il6*$^{RD/wt}$ mice on day 7 after immunization as in **a**, followed by treatment with anti-Thy1.1 (monoclonal antibody 19E12; bottom row), for the depletion of IL-6$^+$ (Thy1.1$^+$) DCs, or with isotype-matched control antibody (mouse IgG2a; top row), and re-stimulation of the cells *ex vivo* with PMA and ionomycin. (**e**) EAE in mice treated with anti-Thy1.1 or control antibody as in **d** (key) at various times (horizontal axes) after immunization as in **a**. (**f**) EAE in wild-type mice (WT), *Il6*$^{flox/flox}$ mice and *Il6*$^{\Delta DC}$ mice (key) at various times (horizontal axes) after immunization as in **a**. *$P < 0.05$ (analysis of variance (ANOVA) plus Fisher's LSD test). Data are from one experiment representative of two experiments (**a**–**d**; mean ± s.d. of $n = 4$ mice in **b**; five mice per group in **d**) or are representative of two experiments (**e**; mean ± s.e.m. of $n = 6$ mice per group) or four experiments (**f**; mean ± s.e.m. of $n = 7$ mice per group).

a published STAT3-dependent gene set[16], expression of STAT3 target genes was overrepresented in the expression profile of 2D2 T cells primed in *Il6*$^{flox/flox}$ mice relative to their representation in the profile of 2D2 T cells primed in *Il6*$^{\Delta DC}$ mice (**Supplementary Fig. 6** and **Supplementary Table 4**). Thus, we next directly assessed the activation of STAT3 in T cells in *Il6*$^{flox/flox}$, *Il6*$^{-/-}$ or *Il6*$^{\Delta DC}$ mice. Naive 2D2

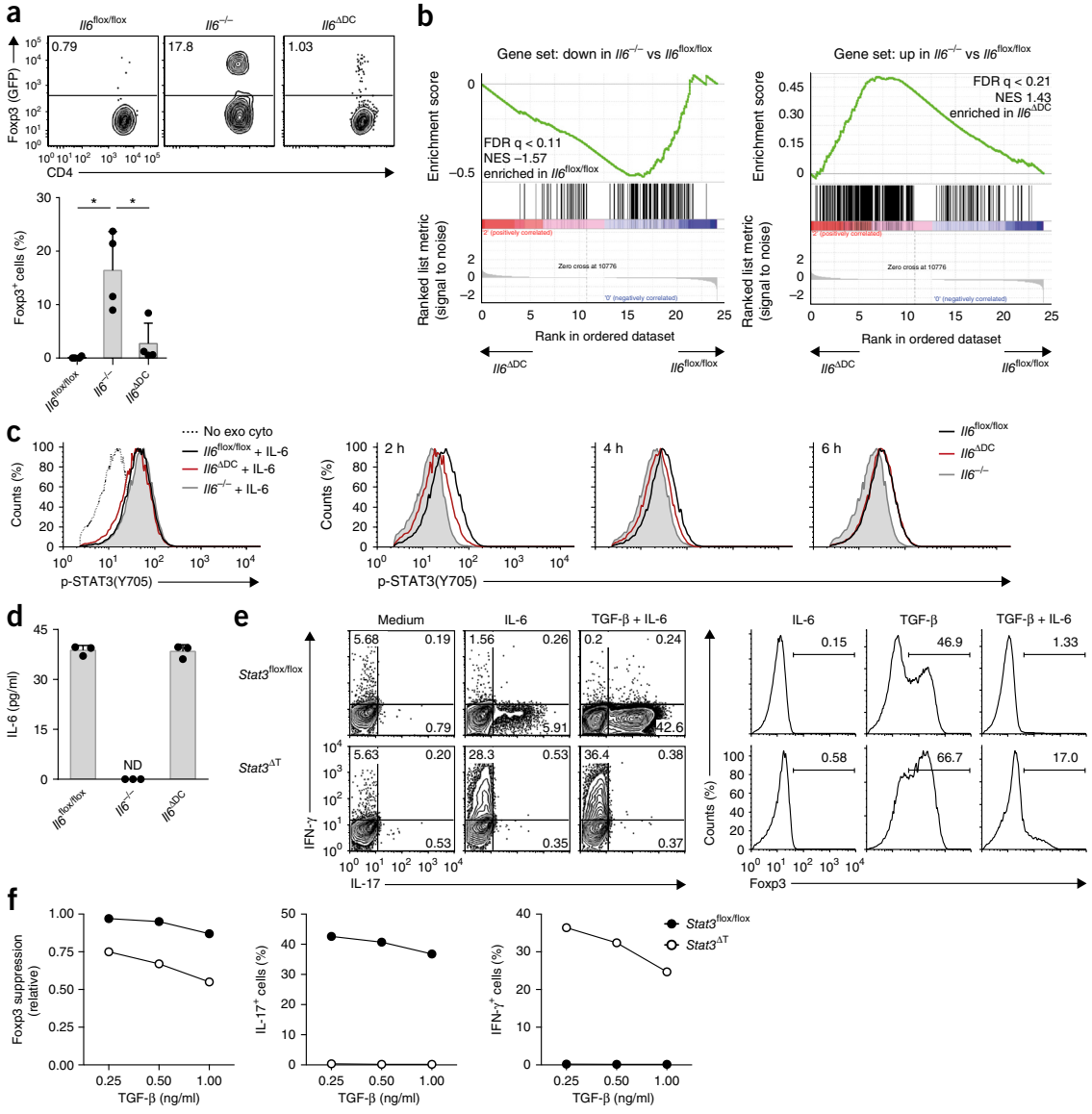

Figure 2 Conditional ablation of *Il6* in DCs results in delayed activation of STAT3 in antigen-specific T cells but does not impair the suppression of Foxp3 induction. (**a**) Flow cytometry (top) of donor cells isolated from the draining lymph nodes of *Il6*$^{flox/flox}$ (control) hosts, *Il6*$^{-/-}$ hosts or *Il6*$^{\Delta DC}$ hosts (above plots) given transfer of naive MOG(35–55) specific T cells from 2D2 × *Foxp3gfp.*KI donors, followed by immunization of the hosts with MOG(35–55) and analysis, 3 weeks later, of Foxp3 (GFP) expression; below, frequency of Foxp3$^+$ cells among 2D2 (donor) cells. (**b**) Gene-set–enrichment analysis of IL-6 target gene sets (above plots) in the gene-expression profile (RNA-sequencing analysis) of Foxp3$^-$ 2D2 T cells derived from *Il6*$^{flox/flox}$ control or *Il6*$^{\Delta DC}$ host mice as in **a**. Above plots: genes downregulated (left) or upregulated (right) in 2D2 T cells primed in *Il6*$^{-/-}$ mice relative to their expression in 2D2 T cells primed in *Il6*$^{flox/flox}$ mice. FDR, false-discovery rate; NES, normalized enrichment score. (**c**) Phosphorylation of STAT3 at Tyr705 (p-STAT3(Y705)) in 2D2 T cells cultured *in vitro*, together with splenocytes from *Il6*$^{flox/flox}$, *Il6*$^{-/-}$ or *Il6*$^{\Delta DC}$ mice (key), in the presence of MOG(35-55) and a matrix metalloproteinase inhibitor (to block shedding of IL-6Rα), with the addition of no additional cytokines (No exo cyto) or exogenous recombinant IL-6 (key) (left), or assessed at 2 h, 4 h or 6 h (above plots) after the addition of LPS (right). (**d**) IL-6 in supernatants of co-cultures of 2D2 T cells and splenocytes (as in **c**, right), assessed 2 h after the addition of LPS. ND, not detected. (**e**) Flow cytometry of naive T cells obtained from *Stat3*$^{flox/flox}$ (control) mice or CD4-Cre × *Stat3*$^{flox/flox}$ mice (*Stat3*$^{\Delta T}$) and activated with anti-CD3 and anti-CD28 in the presence of no additional treatment (Medium), IL-6 alone, or TGF-β plus IL-6 (above plots), followed by stimulation with PMA and ionomycin and intracellular cytokine staining (left) or nuclear staining of Foxp3 in CD4$^+$ T cells (right) on day 3 of culture. Numbers above bracketed lines (right) indicate percent Foxp3$^+$ cells. (**f**) Suppression of Foxp3 expression (left) and frequency of IL-17$^+$ cells (middle) or IFN-γ$^+$ cells (right) among CD4$^+$ cells, assessed in naive *Stat3*$^{flox/flox}$ (control) and *Stat3*$^{\Delta T}$ CD4$^+$ T cells as in **e** (key) treated with IL-6 (50 ng/ml) and graded concentrations (horizontal axes) of TGF-β; results at left are presented as those in cells treated with TGF-β – those in cells treated with TGF-β plus IL-6 / those in cells treated with TGF-β. Each symbol **a**,**d** represents an individual mouse (**a**) or supernatant (**d**). *$P < 0.005$ (ANOVA plus Tukey's test). Data are representative of two experiments (**a**,**c**,**d**; mean + s.d. of $n = 4$ (**a**) or $n = 3$ (**d**) mice per genotype), one experiment with three mice per genotype (**b**) or three experiments (**e**,**f**).

T cells were co-cultured with *Il6*$^{flox/flox}$, *Il6*$^{-/-}$ or *Il6*$^{\Delta DC}$ splenocytes in the presence of the cognate antigen MOG(35–55). After stimulation of the cells with lipopolysaccharide (LPS), activation of STAT3 was negligible in T cells cultured with *Il6*$^{-/-}$ APCs (**Fig. 2c**). The activation of STAT3 was delayed in T cells primed with *Il6*$^{\Delta DC}$ APCs relative to its activation in T cells primed with *Il6*$^{flox/flox}$ APCs (**Fig. 2c**), despite the presence of similar amounts of soluble IL-6 in the supernatants of *Il6*$^{flox/flox}$ APC–T cell or *Il6*$^{\Delta DC}$ APC–T cell co-cultures (**Fig. 2d**). Thus, IL-6 induced early and robust activation of STAT3 in antigen-specific 2D2 T cells only when provided by DCs.

In addition, because the *in vivo* priming of 2D2 T cells in *Il6*$^{\Delta DC}$ mice resulted in a highly efficient suppression of Foxp3 induction (**Fig. 2a**), we investigated whether the activation of STAT3 had differential effects on the IL-6-mediated suppression of Foxp3 expression and the induction of effector properties in conventional T cells. Naive CD44$^-$CD25$^-$CD4$^+$ T cells from *Stat3*$^{flox/flox}$ (control) mice or CD4-Cre × *Stat3*$^{flox/flox}$ mice (with T cell–specific deficiency in STAT3) were activated *in vitro* with anti-CD3 and anti-CD28 in the presence of TGF-β with or without IL-6, followed by assessment of induction of the expression of Foxp3 and effector cytokines. As expected, STAT3 was indispensable for the induction of IL-17 expression (**Fig. 2e**). However, STAT3-deficient T cells had high expression of IFN-γ when differentiated under T_H17-polarizing conditions (**Fig. 2e**,**f**). The TGF-β-induced expression of Foxp3 was suppressed (at least in part) by IL-6 in STAT3-deficient T cells (**Fig. 2e**,**f**), which indicated that a lack of STAT3 in T cells resulted in a T_H1-cell-like phenotype under T_H17-differentiation conditions. In summary, these data suggested that T cells were able to distinguish between DC-derived IL-6 and IL-6 from other sources via different STAT3-activation kinetics, which resulted in different T cell phenotypes.

IL-6 cluster signaling is an efficient signaling mode

Beyond classic IL-6 signaling through the binding of soluble IL-6 (sIL-6) to its membrane-bound receptor, soluble IL-6–IL-6Rα complexes engage gp130 on target cells that lack IL-6Rα through the process of IL-6 trans-signaling[13]. We investigated whether during a cognate DC–T cell encounter, DC-bound IL-6Rα trans-presents DC-derived IL-6 to T cells through a distinct IL-6 trans-presentation process that requires the clustering of donating cells and receiving cells (IL-6 cluster signaling). First, we established the functionality of IL-6 cluster signaling through stable retroviral expression, in Ba/F3 cells (an IL-3-dependent mouse pro-B-cell line that lacks both endogenous IL-6Rα and gp130 expression[17,18]), of either IL-6Rα (lacking enhanced GFP (eGFP); thus, the cells (Ba/F3–IL-6Rα) show no GFP fluorescence) or gp130-eGFP (Ba/F3–gp130-eGFP; cells appear bright green), followed by analysis of their proliferative response to IL-6 signaling (**Fig. 3a**). While in separate cultures, Ba/F3–IL-6Rα cells (which lacked gp130) did not proliferate in response to either sIL-6 or a sIL-6–sIL-6Rα complex (called 'hyper-IL-6' here)[19], Ba/F3–gp130-eGFP cells (which lacked IL-6Rα) proliferated in response to hyper-IL-6 but not in response to sIL-6 (**Fig. 3a**); this suggested that hyper-IL-6 formed a functional signaling complex with membrane bound gp130-eGFP in the Ba/F3–gp130-eGFP cells. Notably, when Ba/F3–gp130-eGFP cells were co-cultured with Ba/F3–IL-6Rα cells, sIL-6 alone induced the proliferation of Ba/F3–gp130-eGFP cells (**Fig. 3b**,**c**), which suggested that the Ba/F3–IL-6Rα cells trans-presented IL-6 to the Ba/F3–gp130-eGFP cells and induced proliferation of the latter cells. This IL-6 cluster signaling required the clustering of Ba/F3–IL-6Rα cells and Ba/F3–gp130-eGFP cells in the same co-culture. Exogenous anti-IL-6Rα neutralized IL-6 cluster signaling, but soluble gp130 linked to the crystallizable fragment Fc (sgp130-Fc), a strong inhibitor of IL-6 trans-signaling by hyper-IL-6, did not (**Fig. 3b**); this indicated a functional difference between IL-6 trans-signaling and IL-6 cluster signaling. Together, these results suggested that IL-6 bound to IL-6Rα on the surface of IL-6Rα-expressing cells signaled through membrane-bound gp130 in cells that did not express IL-6Rα, when both cell types were in physical proximity.

DCs present IL-6 *in trans* and induce IL-6 cluster signaling

Next we assessed the ability of DCs to present IL-6 *in trans* during a cognate interaction with T cells (**Supplementary Fig. 7**). Naive (CD4$^+$CD44$^-$GFP$^-$ (Foxp3$^-$)) 2D2 T cells were co-cultured with BMDCs in the presence of the cognate antigen MOG(35–55) and LPS to induce IL-6 production in BMDCs. GFP$^-$ (Foxp3$^-$) effector 2D2 T cells showed robust activation of STAT3, as assessed by flow cytometry, when they were co-cultured with wild-type BMDCs but not after co-culture with *Il6ra*$^{-/-}$ BMDCs, although the amount of soluble IL-6 produced by wild-type BMDCs and *Il6ra*$^{-/-}$ BMDCs was similar (**Fig. 4a**,**b**). To determine if IL-6 cluster signaling occurred during cognate DC–T cell interactions, we co-cultured wild-type BMDCs with naive T cells isolated from either *Il6ra*$^{flox/flox}$ (control) mice or CD4-Cre × *Il6ra*$^{flox/flox}$ mice (with conditional deficiency in IL-6Rα in T cells (*Il6ra*$^{\Delta T}$)) and treated the cells with staphylococcal enterotoxin B (SEB), a superantigen that activates T cells that express a TCR with β-chain variable region 8 ($V_β8^+$ T cells) and does so in a manner dependent on major histocompatibility complex class II (ref. 20). $V_β8^+$ T cells had a more intense signal for phosphorylated (activated) STAT3 than that of $V_β8^-$ T cells present in the same culture (**Fig. 4c**). In addition, activation of STAT3 occurred in both IL-6Rα-sufficient (control) $V_β8^+$ T cells and *Il6ra*$^{\Delta T}$ $V_β8^+$ T cells (**Fig. 4c**). In contrast, exogenous soluble IL-6 induced phosphorylation of STAT3 in IL-6Rα-sufficient (control) T cells but not in *Il6ra*$^{\Delta T}$ T cells (**Fig. 4c**). In addition, when 2D2 T cells (with transgenic expression of a TCR specific for MOG(35–55)) and OT-II T cells (with transgenic expression of a TCR specific for the epitope OVA(323–339) (ovalbumin amino acids 323–339)) were co-cultured with wild-type BMDCs in a triple culture, early phosphorylation of STAT3 was observed exclusively in T cells whose cognate antigen was present in the culture but not in the co-cultured T cells of irrelevant specificity (**Fig. 4d**,**e**); this suggested that IL-6 cluster signaling did not result in the bystander activation of T cells that did not interact with the DCs in a cognate manner.

To further characterize IL-6 cluster signaling during a DC–T cell interaction, we used a variety of IL-6-blocking reagents at the time of LPS activation of BMDCs co-cultured with 2D2 T cells in the presence of MOG(35–55). The monoclonal antibody MR16-1, which binds IL-6Rα, completely abolished the phosphorylated STAT3 signal in the 2D2 T cells (**Fig. 4f**). In contrast, sgp130-Fc did not inhibit the phosphorylation of STAT3 in the 2D2 T cells (**Fig. 4f**), which indicated that sgp130-Fc was unable to engage the membrane-bound IL-6–IL-6Rα complex interacting with gp130 *in trans*. In addition, antibodies to IL-6, and in particular mAb#8, a monoclonal antibody to IL-6 that binds the interaction site between IL-6 and IL-6Rα[10], failed to block the activation of STAT3 in T cells in response to LPS-activated BMDCs with which the T cells were co-cultured (**Fig. 4f**).

Because IL-6 bound in a complex with IL-6Rα would be less easily neutralized by antibodies to IL-6, we investigated whether IL-6 was loaded onto IL-6Rα in the intracellular compartment and transported to the cell membrane of DCs as a complex. We incubated mixtures of equal numbers of *Il6ra*$^{-/-}$ BMDCs and wild-type BMDCs or of *Il6ra*$^{-/-}$ BMDCs and *Il6*$^{-/-}$ BMDCs with naive (CD44$^-$ GFP$^-$ (Foxp3$^-$)) 2D2 T cells in the presence of MOG(35–55) and stimulated

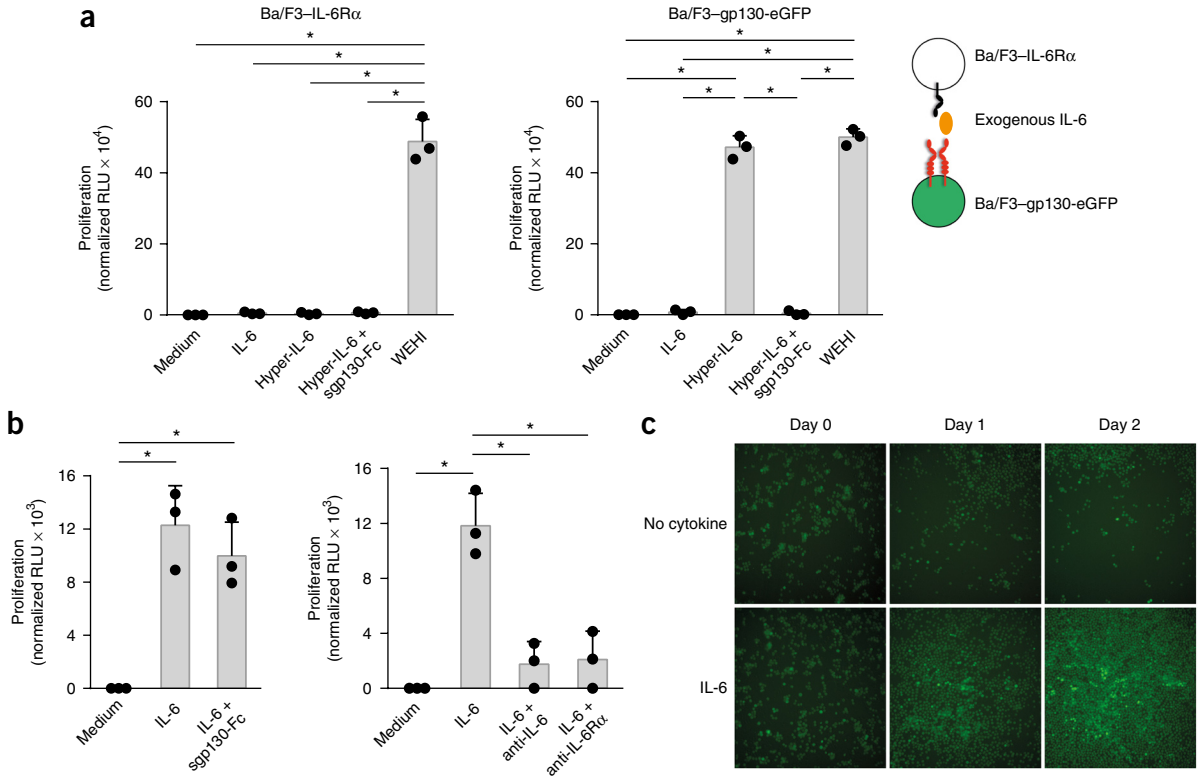

Figure 3 Presentation of IL-6 *in trans* is a functional IL-6 signaling modality in Ba/F3 cells and is not blocked by sgp130-Fc. (**a**) Proliferative response of Ba/F3–IL-6Rα cells (left) or Ba/F3–gp130-eGFP cells (right) cultured (separately, in equal amounts) for 2 d with human IL-6 (10 ng/ml), hyper-IL-6 (10 ng/ml), hyper-IL-6 (10 ng/ml) plus sgp130-Fc (1 μg/ml) or 1% IL-3-containing supernatants conditioned by WEHI-3 mouse leukemia cells (WEHI) or left untreated (Medium); results are presented as relative light units (RLU), normalized to those of cells cultured in medium alone. Far right, structure of Ba/F3–IL-6Rα and Ba/F3–gp130-eGFP in complex with IL-6. (**b**) Proliferative response of Ba/F3–IL-6R and Ba/F3–gp130-eGFP cells cultured together for 2 d (at a ratio of 1:10) and left untreated (Medium) or stimulated with IL-6 (10 ng/ml), IL-6 (10 ng/ml) plus sgp130-Fc (1 μg/ml), IL-6 (10 ng/ml) plus anti-IL-6 (mAb#8; 1 μg/ml), or IL-6 (10 ng/ml) plus anti-IL-6Rα (tocilizumab; 1 μg/ml); results presented as in **a**. (**c**) Microscopy of Ba/F3–IL-6R and Ba/F3–gp130-eGFP cells cultured together (at a ratio of 1:10) for 0–2 d (above images) in the presence (bottom row) or absence (No cytokine) of IL-6 (10 ng/ml). Original magnification, ×10. Each symbol (**a**,**b**) represents an individual sample. $^*P < 0.05$ (ANOVA plus Tukey's multiple-comparisons test). Data are representative of three experiments (mean ± s.d. of $n = 3$ samples in **a**,**b**).

the cultures with LPS. Within 120 min of LPS stimulation, the culture of *Il6ra*$^{-/-}$ BMDCs plus wild-type BMDCs elicited substantial activation (phosphorylation) of STAT3 in GFP$^-$ (Foxp3$^-$) effector T cells, while the culture of *Il6ra*$^{-/-}$ BMDCs plus *Il6*$^{-/-}$ BMDCs failed to induce early substantial phosphorylation of STAT3 in T cells, similar to 'pure' *Il6ra*$^{-/-}$ BMDCs (without *Il6*$^{-/-}$ BMDCs) cultured with naive 2D2 T cells (**Fig. 4g**); this indicated that the *Il6*$^{-/-}$ BMDCs, which expressed IL-6Rα, did not 'pick up' the ambient IL-6 supplied by the *Il6ra*$^{-/-}$ BMDCs and did not trans-present ambient IL-6 to T cells. Notably, the interaction of BMDCs with T cells did not result in substantial phosphorylation of STAT3 in BMDCs within 120 min (**Fig. 4h**), which suggested that gp130 in the BMDCs did not sense the DC-bound IL-6–IL-6Rα complex *in cis*. However, there was only 'smoldering' activation of STAT3 in BMDCs beyond 120 min of LPS stimulation (**Fig. 4h**). The late activation (phosphorylation) of STAT3 in BMDCs was greater in the cultures of *Il6ra*$^{-/-}$ BMDCs plus wild-type BMDCs than in the cultures of *Il6ra*$^{-/-}$ BMDCs plus *Il6*$^{-/-}$ BMDCs (**Fig. 4h**), which suggested that the larger amount of soluble IL-6 in the cultures of *Il6ra*$^{-/-}$ BMDCs plus wild-type BMDCs (data not shown) was responsible for classic IL-6 signaling into BMDCs beyond 120 min after LPS stimulation. Thus, DCs loaded IL-6 onto IL-6Rα in their intracellular compartment and used the IL-6–IL-6Rα complex to perform IL-6 cluster signaling when cognately interacting with T cells. IL-6 cluster signaling then led to the targeted activation of STAT3 in antigen-specific T cells but not in bystander T cells.

Co-localization of IL-6 and IL-6Rα in DCs

Next we used confocal microscopy to visualize IL-6–IL-6Rα complexes in BMDCs that interacted with 2D2 T cells in a cognate manner. BMDCs were co-cultured with 2D2 T cells in the presence of MOG(35–55) and were stimulated with LPS in the absence of exogenous IL-6. We detected 'clustered' IL-6 on the surface of LPS-stimulated BMDCs interacting with 2D2 T cells, with some IL-6 located at the BMDC–T cell interaction interface (**Fig. 5a**). To determine whether IL-6 and IL-6Rα interact on the surface of BMDCs, we performed a proximity-ligation assay (PLA)[21]. IL-6-deficient, IL-6Rα-deficient or wild-type BMDCs were co-cultured with 2D2 T cells in the presence of MOG(35–55) and stimulated with LPS. IL-6 and IL-6Rα were simultaneously labeled by antibodies, followed by PLA for the visualization of IL-6–IL-6Rα complexes. We detected positive PLA signals indicative of the co-localization of IL-6 and IL-6Rα at a distance of less than 40 nm in wild-type BMDC–T cell co-cultures (**Fig. 5b**), while we observed only few PLA signals in *Il6*$^{-/-}$ or *Il6ra*$^{-/-}$ BMDC–T cell co-cultures (**Fig. 5b**,**c**); this suggested that the background of nonspecific PLA-amplification reactions was low. Co-localization of IL-6 and IL-6Rα occurred in the cytoplasm and at the membrane

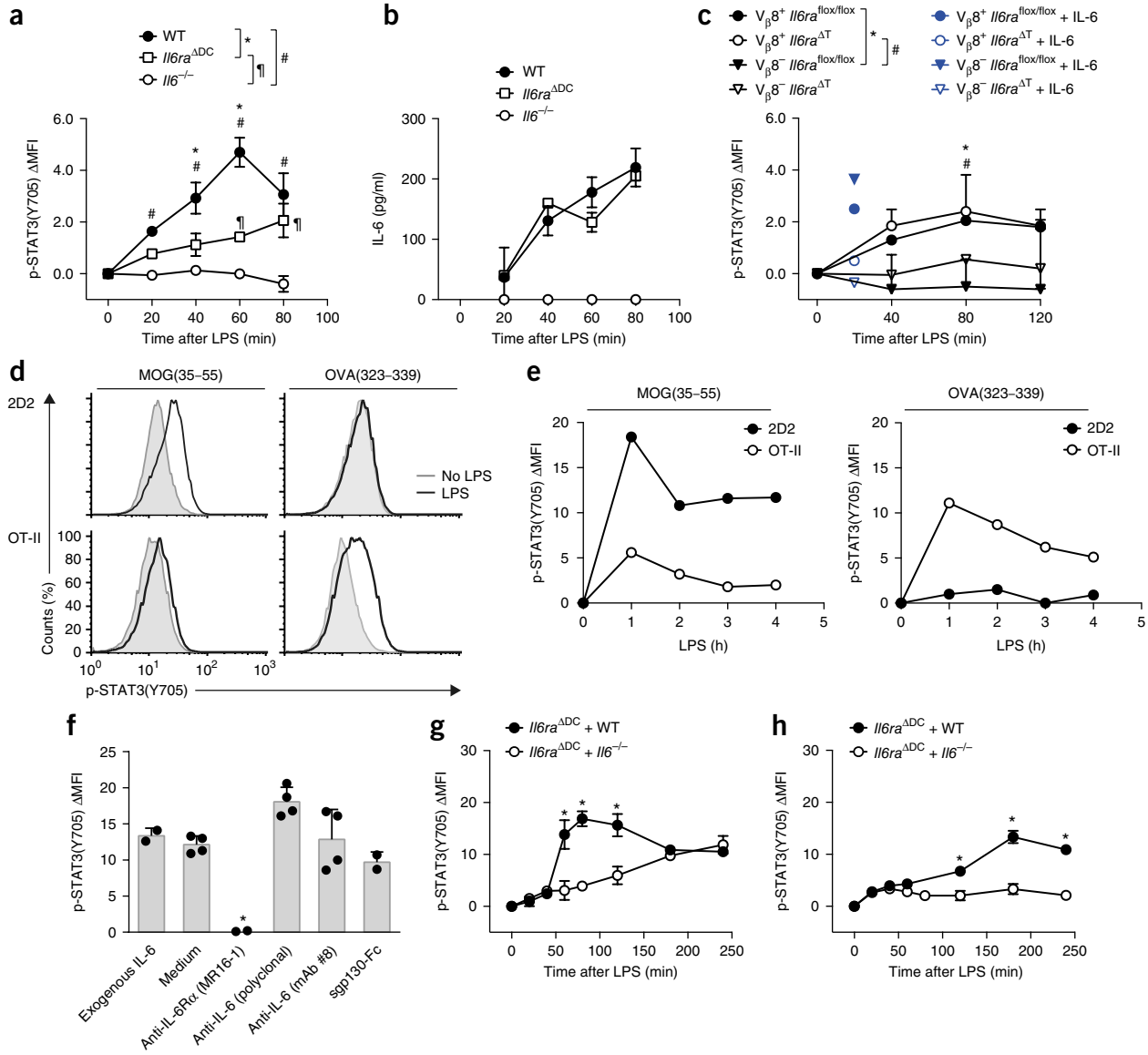

Figure 4 DCs perform IL-6 cluster signaling during antigen specific-priming of T cells. (**a**) Phosphorylation of STAT3 at Tyr705 in 2D2 T cells cultured with wild-type, *Il6*$^{-/-}$ or *Il6ra*$^{\Delta DC}$ BMDCs (key) in the presence of MOG(35–55) and stimulated for various times (horizontal axis) with LPS; results are presented as mean florescence intensity relative to that at time 0 (ΔMFI) throughout. (**b**) ELISA of IL-6 in supernatants of cells as in **a**. (**c**) Phosphorylation of STAT3 at Tyr705 in $V_\beta8^-$ or $V_\beta8^+$ T cells generated by the culture of *Il6ra*$^{flox/flox}$ or *Il6ra*$^{\Delta T}$ CD4$^+$ T cells (key) with wild-type BMDCs in the presence of SEB, followed by stimulation with LPS (left key), or in such cells cultured in the presence of exogenous IL-6 (right key). (**d**,**e**) Phosphorylation of STAT3 at Tyr705 in 2D2 or OT-II T cells (left margin (**d**) or key (**e**)) from triple cultures of wild-type BMDCs, 2D2 T cells and OT-II T cells stimulated with MOG(35–55) (left) or OVA(323–339) (right) and assessed at 2 h (**d**) or various times (horizontal axes; **e**) after the addition of LPS. (**f**) Phosphorylation of STAT3 at Tyr705 in 2D2 T cells cultured for 2 h with wild-type BMDCs and MOG(35–55) in the presence of exogenous IL-6, LPS alone (Medium), or LPS and anti-IL-6Rα (MR16-1), anti-IL-6 (polyclonal antibody or mAb#8) or sgp130-Fc (1 μg/ml each). Each symbol represents an individual sample. (**g**,**h**) Phosphorylation of STAT3 at Tyr705 in 2D2 T cells (**g**) or BMDCs (**h**) from co-cultures of 2D2 T cells with various mixtures of BMDCs (keys). *,¶,#$P < 0.05$ (ANOVA plus Tukey's multiple-comparisons test). Data are representative of four experiments (**a**,**b**,**f**; mean ± s.d. of $n = 2$ samples (**a**,**b**) or mean + s.d. of $n = 4$ samples (**f**)), two experiments (**c**–**e**; mean + s.d. of $n = 2$ samples in **c**) or three experiments (**g**,**h**; mean ± s.d. of $n = 2$ samples).

surface of wild-type BMDCs, with some signal localized at the DC–T cell interaction zone (*xz* projections, **Fig. 5b**). Thus, we were able to visualize DC-associated IL-6–IL-6Rα complexes in DCs.

IL-6 cluster signaling during antigen-specific T cell priming *in vivo*

Next we investigated whether a lack of DC-mediated IL-6 cluster signaling could explain the lack of EAE development in *Il6*$^{\Delta DC}$ mice. CD11b$^+$ DCs isolated from the draining lymph nodes of wild-type mice immunized with MOG(35–55) in CFA showed surface and intracellular expression of IL-6Rα (**Fig. 6a** and **Supplementary Fig. 7**). In CD11c-Cre × *Il6*$^{RD/wt}$ × R26 *Stop*$^{flox/flox}$ YFP mice immunized the same way, the surface expression of IL-6Rα was higher in Thy1.1$^+$ (IL-6$^+$) DCs isolated from the draining lymph nodes than in their Thy1.1$^-$ counterparts (**Fig. 6b**), which indicated that DCs that expressed IL-6Rα and IL-6 simultaneously could be detected in the draining lymph nodes of the immunized mice. To investigate the requirement for DC-mediated IL-6 cluster signaling in the priming of pathogenic T cells *in vivo*, we immunized *Il6ra*$^{\Delta DC}$ mice, which

lack IL-6Rα specifically in DCs and are thus unable to *trans*-present IL-6 during antigen specific priming, with MOG(35–55) in CFA. In contrast to *Il6ra*$^{flox/flox}$ (control) mice, *Il6ra*$^{\Delta DC}$ mice were resistant to EAE (**Fig. 6c**). Thus, IL-6 cluster signaling was needed to promote the differentiation of pathogenic T cells during antigen-specific priming in a DC-proximal manner.

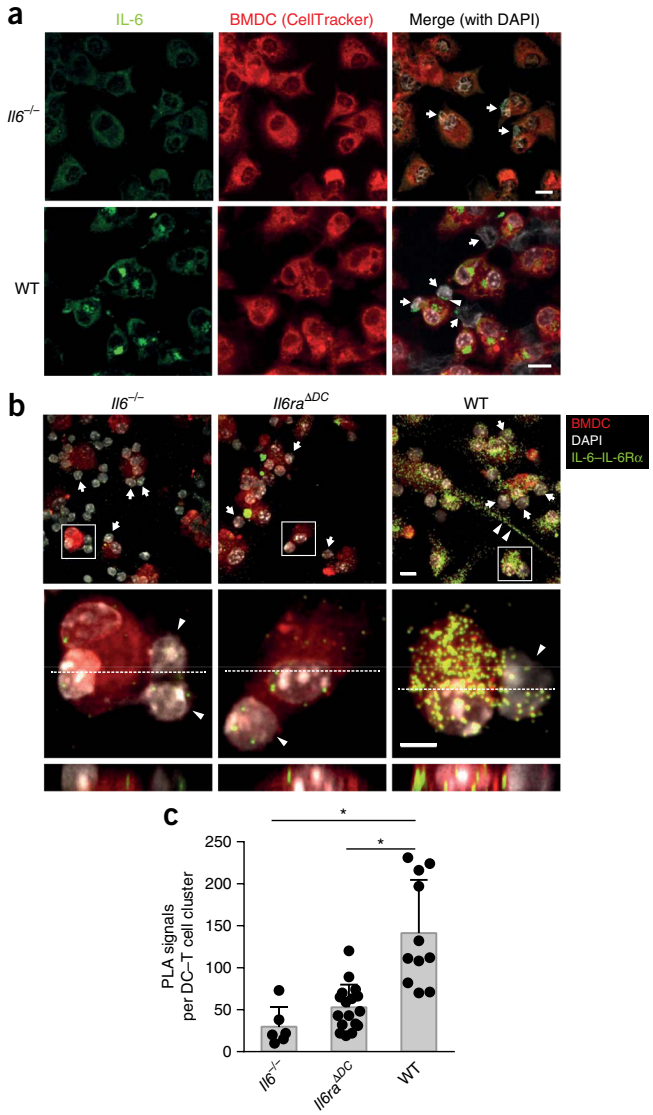

Figure 5 The IL-6–IL-6Rα complex is formed in intracellular compartments of DCs and is presented *in trans* to cognately interacting T cells. (**a**) Immunofluorescence staining of IL-6 (green) in 2D2 T cells (arrows) and *Il6*$^{-/-}$ BMDCs (top row) or wild-type BMDCs (bottom row) pre-stained with fluorescent dye (CellTracker), cultured together in the presence of MOG(35–55), stimulated for 80 min with LPS, then fixed and permeabilized: arrowhead, IL-6 signal at the DC–T cell interface; white, nuclei stained with the DNA-binding dye DAPI. Scale bars, 10 μm. (**b**) PLA of IL-6–IL-6Rα interactions (green) in BMDCs interacting with 2D2 T cells cultured together with wild-type, *Il6*$^{-/-}$ or *Il6ra*$^{-/-}$ BMDCs (above images) pre-stained with fluorescent dye as in **a**, followed by LPS stimulation and fixation and permeabilization, assessed by confocal microscopy (top row) showing nuclei (DAPI), BMDCs (CellTracker), IL-6–IL-6Rα complexes (green), T cells (arrows) and a cytoplasmic bridge of a wild-type DC (arrowheads); middle and bottom, enlargement of areas outlined above, showing DC–T cell interactions (arrowheads) in the *xy* plane (middle), or the *xz* plane (bottom). Scale bars, 10 μm (top) or 5 μm (middle and bottom). (**c**) Quantification of IL-6–IL-6Rα complexes (PLA signals) per DC–T cell cluster in cultures as in **b**. Each symbol represents an individual signal dot per cluster. *$P < 0.0001$ (ANOVA plus Tukey's post-test). Data are representative of four experiments (**a**) or two experiments (**b**,**c**; mean + s.d. in **c**).

To assess the expression of IL-6Rα on T cells *in vivo*, we sorted naive (CD44$^-$ GFP$^-$ (Foxp3$^-$)) T cells from 2D2 × *Foxp3gfp*.KI mice, transferred the cells into congenic (CD45.1$^+$) host mice and then immunized host mice with MOG(35–55) in CFA. The transferred cells showed downregulation of the surface expression of IL-6Rα in the draining lymph nodes from day 1 after immunization through at least day 5, when engaged in an antigen-specific encounter, as defined by upregulation of expression of the activation markers CD69 (day 1) or CD25 (day 5) (**Fig. 6d**). In addition, sgp130-Fc, which blocks IL-6 trans-signaling[22], did not ameliorate EAE in mice with transgenic expression of sgp130-Fc relative to its severity in wild-type (control) mice (**Supplementary Fig. 8**), which indicated that soluble IL-6–IL-6Rα complexes were irrelevant in EAE. We next used mice with conditional deficiency in IL-6Rα in T cells (*Il6ra*$^{\Delta T}$ mice) to investigate whether IL-6Rα-deficient T cells could respond to IL-6 cluster signaling by DCs and become pathogenic effector T cells. We found a greater frequency of Foxp3$^+$ T_{reg} cells in the draining-lymph-node CD4$^+$ T cell compartment of *Il6ra*$^{\Delta T}$ mice immunized with MOG(35–55) in CFA than in that of their *Il6ra*$^{flox/flox}$ (control) counterparts, while *Il6ra*$^{\Delta DC}$ mice immunized with MOG(35–55) had a frequency of Foxp3$^+$ T_{reg} cells similar to that of their *Il6ra*$^{flox/flox}$ (control) counterparts (**Fig. 6e**), consistent with the observation that ambient IL-6, and thus classic IL-6 signaling, provided a significant contribution to suppression of the induction of Foxp3$^+$ T_{reg} cells from conventional T cells in a polyclonal repertoire. Depleting *Il6ra*$^{\Delta T}$ mice of T_{reg} cells (via anti-CD25) before immunization of the mice with MOG(35–55) in CFA led to a greater severity of EAE than that of *Il6ra*$^{\Delta T}$ mice not depleted of T_{reg} cells before such immunization (**Fig. 6f** and **Supplementary Fig. 9**); this indicated that *Il6ra*$^{\Delta T}$ T_H17 cells could be primed to become pathogenic.

Pathogenic T_H17 cells can be differentiated with IL-21 *in vivo* in the absence of IL-6 (refs. 15,23). To evaluate the contribution of IL-21 to the pathogenic priming of T cells in *Il6ra*$^{\Delta T}$ mice, we adoptively transferred naive polyclonal CD4$^+$ T cells from *Il21r*$^{-/-}$ × *Il6ra*$^{\Delta T}$ mice, in which T cells are deficient in the expression of both IL-6Rα and IL-21R, into *Rag1*$^{-/-}$ host mice, which lack endogenous mature T cells and B cells, followed by subcutaneous immunization of the host mice with MOG(35–55) in CFA. *Rag1*$^{-/-}$ mice given transfer of *Il21r*$^{-/-}$ × *Il6ra*$^{\Delta T}$ T cells mounted a T_H17 response in response to this immunization and developed EAE (**Supplementary Fig. 10**). Thus, T cells lacking IL-21 responsiveness and expression of the IL-6Rα that mediates classic IL-6 signaling were still able to become pathogenic T_H17 cells.

Pathogenic T_H17 cells depend on IL-6 cluster signaling

Il6$^{-/-}$ mice develop an exaggerated T_{reg} cell response after antigen-specific priming with adjuvant[15]. Because *Il6*$^{\Delta DC}$ mice showed normal Foxp3$^+$ T_{reg} cell responses but did not develop EAE, we investigated whether effector T cell responses in *Il6*$^{\Delta DC}$ mice were intrinsically inefficient. *Il6*$^{flox/flox}$ (control) mice, *Il6*$^{-/-}$ and *Il6*$^{\Delta DC}$ mice were sensitized with MOG(35–55) in CFA and CD4$^+$Foxp3$^-$ T cells were isolated from the draining lymph nodes for transcriptome analysis. Because EAE is essentially a T_H17 cell–mediated model of CNS autoimmunity, we further assessed a transcriptional module previously associated with 'non-pathogenic' T_H17 cells[8] in Foxp3$^-$ T cells primed in the *Il6*$^{\Delta DC}$ mice. Gene-set–enrichment analysis indicated that conventional Foxp3$^-$ T cells primed in *Il6*$^{\Delta DC}$ mice had a significantly higher expression of *Il6st* (which encodes gp130), *Cd96* and *Eomes* than that of effector T cells primed in a *Il6*$^{flox/flox}$ (control) environment

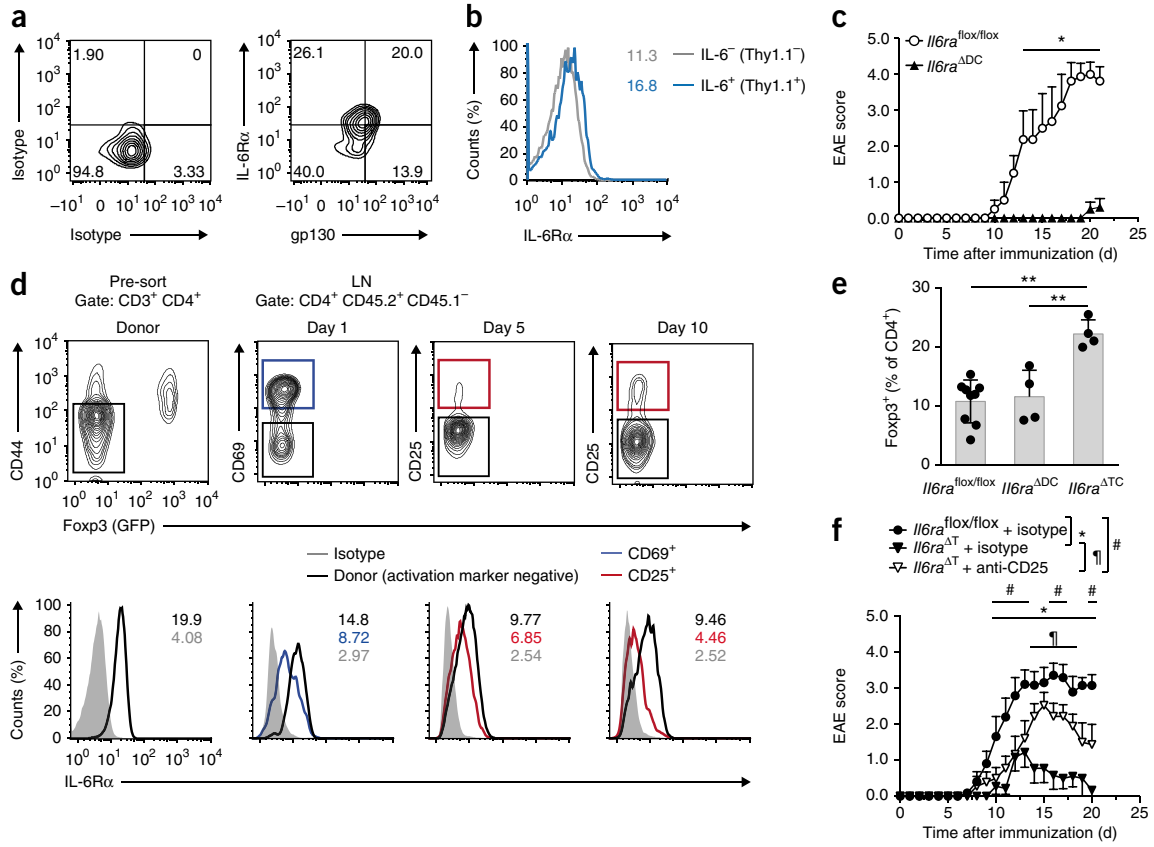

Figure 6 IL-6 cluster signaling is operational *in vivo*. (**a**) Flow cytometry analysis of surface expression of IL-6Rα and gp130 on CD11c$^+$ MHCII^{hi} CD11b$^+$ DCs isolated from the draining lymph nodes of wild-type mice on day 10 after immunization with MOG(35–55) and assessed *ex vivo*. Isotype, isotype-matched control antibodies. (**b**) Surface expression of IL-6Rα on IL-6$^-$ (Thy1.1$^-$) or IL-6$^+$ (Thy1.1$^+$) CD11b$^+$ DCs (key) from the lymph nodes of a CD11c-Cre × *Il6*$^{RD/wt}$ × R26 *Stop*$^{flox/flox}$ YFP mouse treated with cells producing the cytokine Flt3L (as in **Supplementary Fig. 2**), then given injection of LPS, followed by analysis *ex vivo* 2 d later. Numbers in plots indicate the mean florescence intensity of IL-6Rα (colors match key). (**c**) Clinical EAE scores of *Il6ra*$^{flox/flox}$ (control) mice and *Il6ra*$^{\Delta DC}$ mice at various times (horizontal axis) after immunization with MOG(35-55) in CFA. (**d**) Flow cytometry (top) of cells isolated from the draining lymph nodes of wild-type congenic (CD45.1$^+$) host mice given transfer of naive T cells (CD4$^+$CD44$^-$ GFP$^-$ (Foxp3$^-$); gating, far left) from 2D2 × *Foxp3gfp*.KI donor mice, followed by immunization of the host mice with MOG(35–55) and flow cytometry on day 1, 5 or 10 after immunization (above plots), and assessment of surface IL-6Rα expression (bottom) on activated (CD69$^+$ or CD25$^+$) effector (GFP$^-$ (Foxp3$^-$)) 2D2 T cells or non-activated 2D2 T cells (Donor) (key) gated as above. Numbers in plots (bottom row) indicate the mean florescence intensity of IL-6Rα (colors match key). (**e**) Frequency of Foxp3$^+$ T_{reg} cells among CD4$^+$ T cells in the draining lymph nodes of *Il6ra*$^{flox/flox}$ (control) mice, *Il6ra*$^{\Delta DC}$ mice and *Il6ra*$^{\Delta T}$ mice (horizontal axis) after subcutaneous immunization with MOG(35–55) in CFA. Each symbol represents an individual mouse. (**f**) Course of EAE in *Il6ra*$^{flox/flox}$ (control) mice or *Il6ra*$^{\Delta T}$ mice treated with isotype-matched control antibody or depleted of T_{reg} cells by intraperitoneal injection of anti-CD25 (PC61; 0.5 mg) (key) on days 5 and 3 before immunization with MOG(35–55). $^{*,¶,\#}P < 0.05$ and $^{**}P < 0.003$ (ANOVA plus Sidak's post-test (**c**,**f**) or (ANOVA plus Tukey's multiple-comparisons test (**e**)). Data are from one experiment representative of two experiments (**a**,**b**), four experiments (**c**; mean + s.e.m. of $n \geq 4$ mice per genotype) or one experiment (**d**–**f**; $n = 2$ mice per time point (**d**); mean + s.d. of $n \geq 4$ mice per genotype (**e**) or mean ± s.e.m. of $n \geq 9$ mice per group (**f**)).

(**Fig. 7a**,**b**). Notably, CD40L$^+$Foxp3$^-$ T cells primed in the *Il6*$^{\Delta DC}$ mice and re-stimulated with MOG(35–55) *in vitro* exhibited a significantly greater fraction of cells producing only IFN-γ than that of CD40L$^+$ effector T cells primed in *Il6*$^{flox/flox}$ (control) mice (**Fig. 7c**), which indicated that naive T cells primed by IL-6-deficient DCs 'preferentially' differentiated into CD96$^+$IFN-γ$^+$ T cells, which were incapable of inducing EAE.

In vitro, hyper-IL-6 suppressed the upregulation of CD96 expression in IL-6Rα-deficient T cells during T_H17 differentiation (**Fig. 7d**), which indicated that IL-6 presented *in trans* was efficient in preventing the TGF-β-mediated induction of CD96 expression. We used hyper-IL-6 as a surrogate for IL-6 presented *in trans* and compared its effect with that of soluble IL-6 (and thus classic IL-6 signaling) during the APC-free differentiation of naive sorted (CD4$^+$CD44$^-$CD25$^-$) T cells into T_H17 cells. In the presence of an equimolar amount of soluble IL-6 or hyper-IL-6, the induction of IL-17 expression in T cells was similar with each reagent (**Fig. 7e**). However, the suppression of IFN-γ expression during T_H17 differentiation was significantly more efficient with hyper-IL-6 than with soluble IL-6 (**Fig. 7e**). Because under certain conditions Eomes is an inducer of IFN-γ in CD4$^+$ T cells[24,25], we investigated whether the greater fraction of IFN-γ$^+$ T cells induced by TGF-β plus soluble IL-6 was due to high Eomes expression. During T_H17 differentiation, the expression of *Tbx21* mRNA (which encodes the transcription factor T-bet) and, in particular, *Eomes* mRNA was suppressed less efficiently by IL-6 than by hyper-IL-6, with no modulation of the expression of *Rorc* mRNA (which encodes the transcription factor RORγt) (**Fig. 7f**). Conversely, hyper-IL-6 was significantly more potent than soluble IL-6 in inducing robust expression of GFP (IL-23R) during the *in vitro* T_H17 differentiation of naive CD4$^+$ T cells isolated from reporter mice in which a

GFP-reporter-encoding cassette is knocked into the *Il23r* locus (*Il23r*$^{gfp/+}$)[26] (**Fig. 7g,h**). These data indicated that the higher IFN-γ expression in T cells primed in *Il6*$^{\Delta DC}$ mice was linked to lack of IL-6 trans-presentation in these mice.

Because high IFN-γ expression in myelin-specific-T cells is associated with protection against EAE[27], we investigated whether the high IFN-γ expression observed in Foxp3$^-$ effector T cells in the *Il6*$^{\Delta DC}$ mice might determine the resistance of *Il6*$^{\Delta DC}$ mice to EAE. As measured

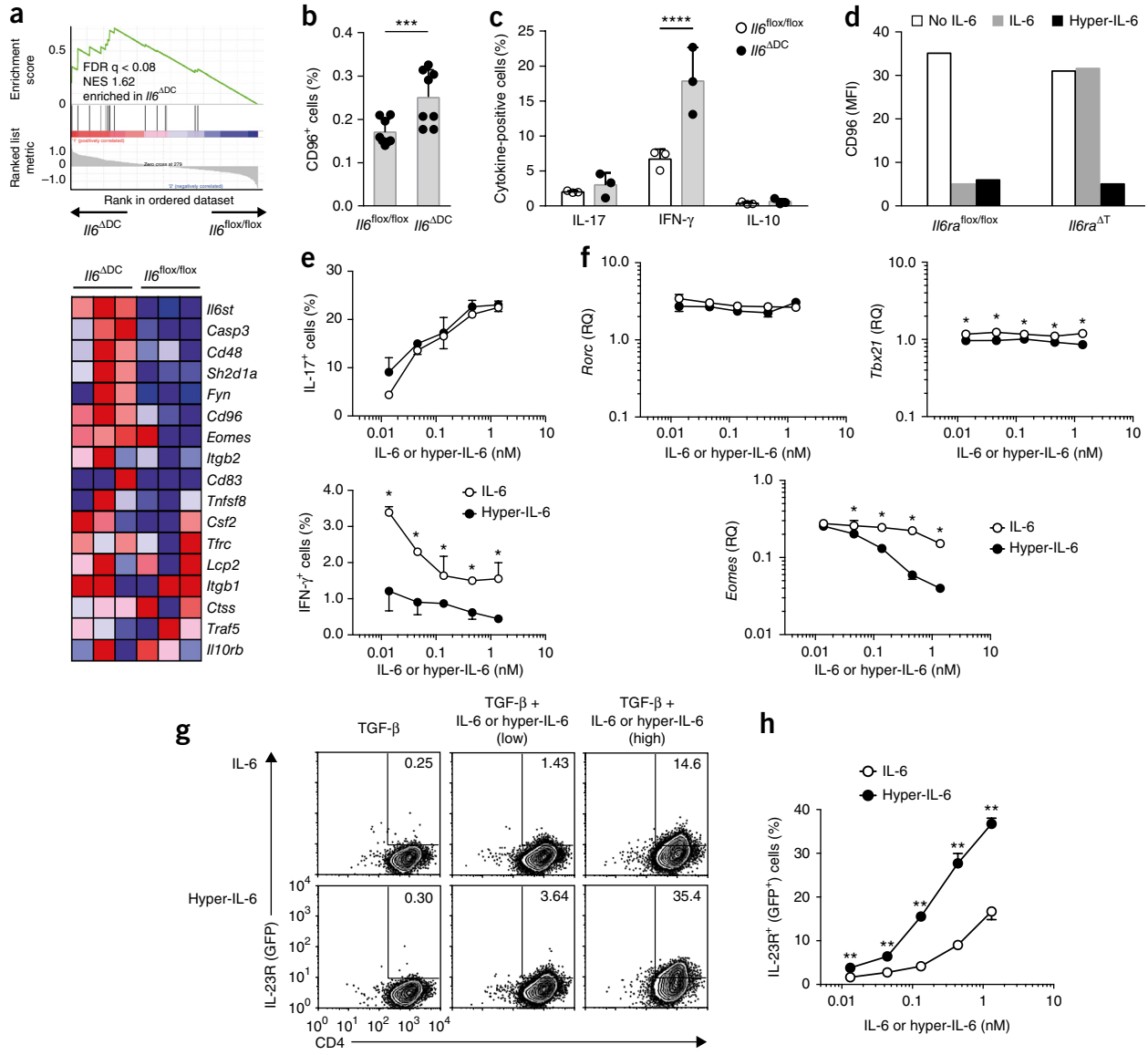

Figure 7 T cell priming is aberrant in an *Il6*$^{\Delta DC}$ environment and results in non-pathogenic T cells. (**a**) Nanostring and gene-set–enrichment analysis of CD4$^+$Foxp3$^-$ T cells purified from the draining lymph nodes of *Il6*$^{\Delta DC}$ and *Il6*$^{flox/flox}$ (control) mice immunized with MOG(35–55) in CFA, presented as an enrichment plot for a known gene set of non-pathogenic T_H17 cells[8] (top), showing genes with higher expression in Foxp3$^-$ T cells from *Il6*$^{\Delta DC}$ mice (left) or *Il6*$^{flox/flox}$ mice (right); below, ranking of genes (right margin) with higher expression in Foxp3$^-$ T cells from *Il6*$^{\Delta DC}$ mice (colors indicate a higher (darker red) or lower (darker blue) *z*-score). (**b**,**c**) Frequency of CD96$^+$ cells (**b**) or cells positive for the intracellular cytokines IL-17, IFN-γ or IL-10 (**c**) among CD40L$^+$ T cells obtained from *Il6*$^{flox/flox}$ (control) mice or *Il6*$^{\Delta DC}$ mice 7 d after immunization with MOG(35–55) and re-stimulated *in vitro* with MOG(35–55). Each symbol represents an individual mouse. (**d**) CD96 expression by naive *Il6ra*$^{flox/flox}$ or *Il6ra*$^{\Delta T}$ T cells (horizontal axis) stimulated in the presence of TGF-β (0.1 ng/ml) plus no IL-6, IL-6 or hyper-IL-6 (key). (**e**) Frequency of IL-17$^+$ cells (top) or IFN-γ$^+$ cells (bottom) among CD4$^+$ T cells generated from naive wild-type T cells activated in the presence of TGF-β and equimolar concentrations (horizontal axes) of soluble IL-6 or hyper-IL-6 (key), followed by re-stimulation with PMA and ionomycin. (**f**) Expression of *Rorc*, *Tbx21* and *Eomes* mRNA in cells activated as in **e** (without re-stimulation); results are normalized to those of the control gene *Actb* and are presented relative to those of cells with no IL-6 (relative expression (RQ)). (**g**) Flow cytometry of naive T cells obtained from IL-23R (*Il23r*$^{gfp/+}$) reporter mice and stimulated for 2 d in the presence of TGF-β alone or TGF-β plus equimolar concentrations (low (0.013 nM) or high (1.3 nM); above plots) of IL-6 or hyper-IL-6 (left margin). Numbers in outlined areas indicate percent GFP$^+$ (IL-23R$^+$) CD4$^+$ T cells. (**h**) Frequency of GFP$^+$ (IL-23R$^+$) cells among CD4$^+$ T cells obtained from mice as in **g** and stimulated for 2 d in the presence of TGF-β with equimolar concentrations (horizontal axes) of IL-6 or hyper-IL-6 (key). $^*P < 0.04$, $^{**}P < 0.03$, $^{***}P = 0.0066$ and $^{****}P < 0.005$ (unpaired *t*-test (**b**), ANOVA plus Sidak's multiple-comparisons test (**c**) or ANOVA plus Holm-Sidak's post-test (**e**,**f**,**h**)). Data are from one experiment (**a**,**b**; three biological replicates (**a**) or mean + s.d. of $n = 8$ mice per genotype (**b**)) or are representative of two experiments (**c**,**d**,**f**–**h**; mean + s.d. of $n = 3$ mice per genotype (**c**) or $n = 3$ samples (**g**,**h**); $n = 2$ samples (**f**)) or three experiments with (**e**; mean ± s.d. of $n = 2$ samples).

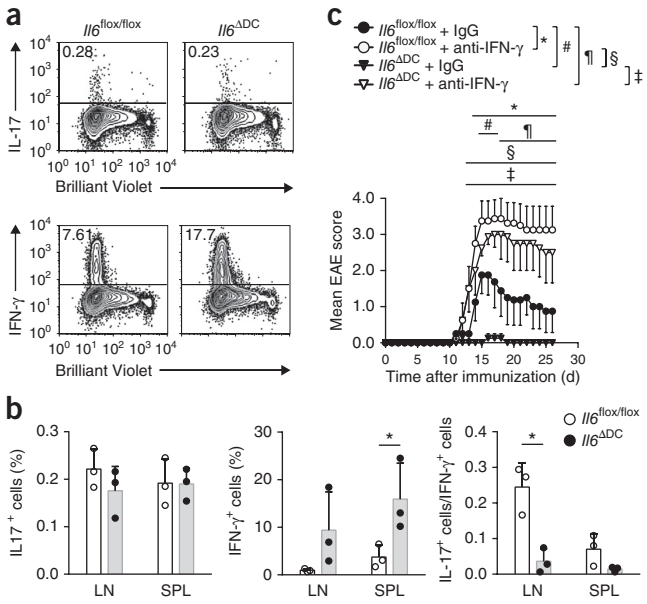

Figure 8 Aberrant priming of T_H17 cells in the absence of DC-mediated IL-6 cluster signaling is reversed by neutralization of IFN-γ *in vivo*. (**a**) Flow cytometry of naive 2D2 T cells labeled with the proliferation dye Brilliant Violet and transferred into *Il6*$^{flox/flox}$ (control) mice or *Il6*$^{\Delta DC}$ mice, followed by immunization of the host mice with MOG(35–55) and isolation of donor cells from the host mice on day 7 after immunization. Numbers in outlined areas indicate percent IL-17$^+$ cells (top row) or IFN-γ$^+$ cells (bottom row). (**b**) Frequency of IL-17$^+$ cells (left) or IFN-γ$^+$ cells (middle), and ratio of IL-17$^+$ cells to IFN-γ$^+$ cells (right), among 2D2 T cells as in **a**. Each symbol represents an individual mouse. (**c**) EAE scores of *Il6*$^{flox/flox}$ (control) and *Il6*$^{\Delta DC}$ mice immunized with MOG(35–55) and given intraperitoneal injection of control antibody (rat IgG1) or 200 μg anti-IFN-γ (key) every other day until day 11 after immunization. $^{*,\#,¶,§,‡}P < 0.04$ (*t*-test (**b**) or ANOVA plus Tukey's post-test (**c**)). Data are representative of two experiments (mean + s.d. (**b**) or mean ± s.e.m. of $n = 4$ mice per group (**c**)).

by dye dilution, 2D2 T cells primed in *Il6*$^{\Delta DC}$ mice proliferated as well as 2D2 T cells primed in *Il6*$^{flox/flox}$ (control) mice did, but the former showed more production of IFN-γ (**Fig. 8a**,**b**). Neutralization of IFN-γ in *Il6*$^{\Delta DC}$ mice with monoclonal antibody to IFN-γ fully restored the susceptibility of *Il6*$^{\Delta DC}$ mice to EAE and resulted in EAE of even greater severity than that of *Il6*$^{flox/flox}$ (control) mice treated with a control antibody (**Fig. 8c**). In summary, these data indicated that priming of T_H17 cells in *Il6*$^{\Delta DC}$ mice in the absence of DC-mediated IL-6 cluster signaling resulted in exaggerated expression of IFN-γ in CD4$^+$ T cells, most probably due to aberrant activation of STAT3 in these cells.

DISCUSSION

Here we found that T cells responded to IL-6 in the absence of IL-6Rα expression through a process that we have called 'IL-6 cluster signaling', in which DC-membrane-bound IL-6Rα in complex with IL-6 was presented *in trans* and was sensed by gp130 molecules expressed on T cells. IL-6 cluster signaling not only replaced classic IL-6 signaling but led to qualitatively different T cell responses. The prototypic cytokine to be trans-presented by auxiliary cells via its high affinity receptor is IL-15 (ref. 28). It is likely that similar to IL-15, IL-6 is loaded onto IL-6Rα in endosomal compartments. Trans-presentation has also been proposed for another member of the IL-6 family, cardiotrophin-like cytokine, through binding to the receptor for ciliary neurotrophic factor[29]. Although IL-6 forms a stable complex with soluble IL-6Rα, the affinity of IL-6 for IL-6Rα is only about 0.5–1 nM (ref. 13) and thus is two orders of magnitude lower than the affinity of IL-15 for IL-15Rα. However, membrane-bound-cytokine trans-presentation has also been reported for IL-2, whose affinity for IL-2Rα is in the same range as the affinity of IL-6 for IL-6Rα[13,30].

During interactions with T cells, DC-mediated IL-6 cluster signaling restricted the IL-6 signal to cognate T cells, with high temporal synchronization with the TCR signal. Such coordination of signals led to the 'imprinting' of pathological properties on the recipient T cells. Notably, suppression of Foxp3 was induced in T cells with diminished or even absent STAT3 signaling and could be fully supported by classic IL-6 signaling. Therefore, the IL-6 that prevented the upregulation of Foxp3 expression in T cells did not have to be derived from the priming DC and could be derived in soluble form from the 'micro-milieu'. Hence, it is possible that the suppression of the induction of Foxp3 expression in T cells occurs as a 'bystander' effect of ambient IL-6. However, the IL-6-dependent induction of inflammatory properties in Foxp3$^-$ T cells is efficient only in the context of antigen presentation and probably does not occur as a bystander effect of ambient IL-6. This suggests that IL-6-mediated pathogenic T cell differentiation passes through two checkpoints: the suppression of Foxp3 induction via classic IL-6 signaling, and the initiation of a pathogenic effector T cell transcriptional program via IL-6 cluster signaling. Therefore, the ability to induce pathogenic T_H17 cells is dependent on APCs that can co-present IL-6 *in trans*.

Here we found that the IL-6$^+$IL-6Rα$^+$ DCs that were able to perform cluster signaling were CD103$^-$ and belonged to the subset of CD11b$^+$Sirpα$^+$ DCs that have been classified as 'cDC2'[31] and have been associated with pathogenic T_H17 responses[32]. As a mechanistic basis for the ability of this DC subset to 'instruct' T_H17 responses is lacking, we propose that IL-6 cluster signaling synchronized with antigen presentation might represent the instructive cue for the development of pathogenic T_H17 cells. IL-6 cluster signaling led to earlier and more robust expression of IL-23R in antigen-activated T cells than did classic IL-6 signaling. Therefore, facilitated sensing of IL-23 further supports their pathogenic phenotype[33]. In contrast, in the absence of IL-6 cluster signaling, IL-23 is unable to compensate for the impaired initiation of a pathogenic transcriptional program in antigen-specific T cells, which suggests that the synchronization of antigen-specific priming and IL-6-mediated STAT3 signaling is fundamental for the pro-inflammatory phenotype of T cells. Because T cell blasts extensively downregulate their surface expression of IL-6Rα, it is plausible that IL-6 cluster signaling is a means of combining a 'pathogenic' IL-6 signal with cognate re-activation. The APC type and the anatomical compartment of this process have not been defined precisely.

We have provided evidence that lack of IL-6 cluster signaling during T_H17 priming deviated the cytokine phenotype into IFN-γ production, which was dependent in part on Eomes expression. Although there has been some controversy in this area[34], IL-6 has been shown to suppress the development of T_H1 cells via direct and indirect mechanisms[35]. Here we demonstrated that IL-6 cluster signaling in particular was an efficient means of preventing the induction of IFN-γ during helper T cell differentiation. In our model, in the absence of IL-6 cluster signaling, insufficient activation of STAT3, and thus a STAT1-STAT3 imbalance, allowed the expression of Eomes and IFN-γ in T_H17-priming conditions and resulted in impaired encephalitogenicity.

Finally, the possibility of IL-6 cluster signaling has implications for therapeutic interventions. Anti-IL-6 failed to inhibit IL-6 cluster signaling. The IL-6–IL-6Rα complex formation occurred within DCs, most probably followed by targeted shuttling to plasma-membrane regions involved in the cognate interaction with T cells, with immediate

accessibility to gp130 molecules on the T cell side. Therefore, site I of the IL-6 molecule[10], which mediates the binding of IL-6 to IL-6Rα and is targeted by most antibodies to IL-6, is already buried in the IL-6–IL-6Rα complex when it appears at the plasma membrane. Although sgp130-Fc suppresses IL-6 trans-signaling[14], IL-6 cluster signaling was not inhibited by sgp130-Fc; we hypothesize that sgp130-Fc cannot access the IL-6–IL-6Rα complex at the DC–T cell interaction zone. However, similar to classic IL-6 signaling and IL-6 trans-signaling, IL-6 cluster signaling remained amenable to neutralization via anti-IL-6Rα. Thus, IL-6-targeting strategies must be carefully re-evaluated for differential signaling modalities in the design of therapeutic strategies for autoimmunity, chronic inflammation and cancer.

METHODS

Methods, including statements of data availability and any associated accession codes and references, are available in the online version of the paper.

Note: Any Supplementary Information and Source Data files are available in the online version of the paper.

ACKNOWLEDGMENTS

We thank all members of the Korn laboratory for input; B. Kunze, B. Lunk and colleagues for mouse care; D. Busch (Technical University of Munich) for OT-II mice (Tg*(TcraTcrb)*^{425Cbn}) expressing the congenic marker CD45.1; F. Greten (Georg-Speyer Haus) for *Stat3*$^{flox/flox}$ (*Stat3*^{tm2Aki}) mice; B. Stockinger (MRC National Institute for Medical Research) for the 19E12 hybridoma; and M. Kopf (ETH, Zürich) for *Il21r*$^{-/-}$ mice. Supported by the Deutsche Forschungsgemeinschaft (TRR128 to A.W. and T.K.; TRR156 and WA1600/8-1 to A.W.; SFB1054-B07 and SyNergy to T.K.; SFB877-A01 to S.R.-J.; SFB877-A10 to C. Gar.; and the cluster of excellence 'Inflammation at interfaces' to S.R.-J. and C. Gar.), the European Research Council (Consolidator Grant 647215 to T.K.), and the Spanish Ministerio de Economía y Competitividad (SAF2011-23272 and SAF2014-56546-R to J.H.).

AUTHOR CONTRIBUTIONS

S.H. designed, performed and analyzed most experiments and drafted the manuscript; N.Y. performed and analyzed key *in vivo* experiments; C. Gar., M.H., L.A., V.H., A.L.C., K.M.-H. and T.R. performed or contributed to specific experiments; C.Gas. performed bioinformatics analysis; H.S.B. and K.S. performed and analyzed nanostring experiments; S.K. and H.B. performed and analyzed RNA-sequencing experiments; B.H., T.M., T.F.W., J.H., M.O., S.R.-J., M.S.-S. provided reagents, advice, design and supervision of experiments; A.W. supervised experiments, analyzed data and wrote the manuscript; and T.K. conceptualized the study, designed and supervised the experiments, analyzed data and wrote the manuscript.

COMPETING FINANCIAL INTERESTS

The authors declare no competing financial interests.

1. Hall, A.O. *et al.* The cytokines interleukin 27 and interferon-γ promote distinct Treg cell populations required to limit infection-induced pathology. *Immunity* **37**, 511–523 (2012).
2. Neufert, C. *et al.* IL-27 controls the development of inducible regulatory T cells and Th17 cells via differential effects on STAT1. *Eur. J. Immunol.* **37**, 1809–1816 (2007).
3. Huber, M. *et al.* IL-27 inhibits the development of regulatory T cells via STAT3. *Int. Immunol.* **20**, 223–234 (2008).
4. Dardalhon, V. *et al.* IL-4 inhibits TGF-β-induced Foxp3$^+$ T cells and, together with TGF-β, generates IL-9$^+$IL-10$^+$Foxp3$^-$ effector T cells. *Nat. Immunol.* **9**, 1347–1355 (2008).
5. Bettelli, E. *et al.* Reciprocal developmental pathways for the generation of pathogenic effector T_H17 and regulatory T cells. *Nature* **441**, 235–238 (2006).
6. Serada, S. *et al.* IL-6 blockade inhibits the induction of myelin antigen-specific Th17 cells and Th1 cells in experimental autoimmune encephalomyelitis. *Proc. Natl. Acad. Sci. USA* **105**, 9041–9046 (2008).
7. Ghoreschi, K. *et al.* Generation of pathogenic T_H17 cells in the absence of TGF-β signalling. *Nature* **467**, 967–971 (2010).
8. Lee, Y. *et al.* Induction and molecular signature of pathogenic T_H17 cells. *Nat. Immunol.* **13**, 991–999 (2012).
9. Gaublomme, J.T. *et al.* Single-cell genomics unveils critical regulators of Th17 cell pathogenicity. *Cell* **163**, 1400–1412 (2015).
10. Boulanger, M.J., Chow, D.-C., Brevnova, E.E. & Garcia, K.C. Hexameric structure and assembly of the interleukin-6/IL-6 alpha-receptor/gp130 complex. *Science* **300**, 2101–2104 (2003).
11. Babon, J.J., Varghese, L.N. & Nicola, N.A. Inhibition of IL-6 family cytokines by SOCS3. *Semin. Immunol.* **26**, 13–19 (2014).
12. Tamura, T. *et al.* Soluble interleukin-6 receptor triggers osteoclast formation by interleukin 6. *Proc. Natl. Acad. Sci. USA* **90**, 11924–11928 (1993).
13. Rose-John, S. & Heinrich, P.C. Soluble receptors for cytokines and growth factors: generation and biological function. *Biochem. J.* **300**, 281–290 (1994).
14. Jostock, T. *et al.* Soluble gp130 is the natural inhibitor of soluble interleukin-6 receptor transsignaling responses. *Eur. J. Biochem.* **268**, 160–167 (2001).
15. Korn, T. *et al.* IL-21 initiates an alternative pathway to induce proinflammatory T_H17 cells. *Nature* **448**, 484–487 (2007).
16. Durant, L. *et al.* Diverse targets of the transcription factor STAT3 contribute to T cell pathogenicity and homeostasis. *Immunity* **32**, 605–615 (2010).
17. Baran, P., Nitz, R., Grötzinger, J., Scheller, J. & Garbers, C. Minimal interleukin 6 (IL-6) receptor stalk composition for IL-6 receptor shedding and IL-6 classic signaling. *J. Biol. Chem.* **288**, 14756–14768 (2013).
18. Palacios, R. & Steinmetz, M. Il-3-dependent mouse clones that express B-220 surface antigen, contain Ig genes in germ-line configuration, and generate B lymphocytes in vivo. *Cell* **41**, 727–734 (1985).
19. Fischer, M. *et al.* I. A bioactive designer cytokine for human hematopoietic progenitor cell expansion. *Nat. Biotechnol.* **15**, 142–145 (1997).
20. White, J. *et al.* The V beta-specific superantigen staphylococcal enterotoxin B: stimulation of mature T cells and clonal deletion in neonatal mice. *Cell* **56**, 27–35 (1989).
21. Söderberg, O. *et al.* Direct observation of individual endogenous protein complexes *in situ* by proximity ligation. *Nat. Methods* **3**, 995–1000 (2006).
22. Linker, R.A. *et al.* IL-6 transsignalling modulates the early effector phase of EAE and targets the blood-brain barrier. *J. Neuroimmunol.* **205**, 64–72 (2008).
23. Nurieva, R. *et al.* Essential autocrine regulation by IL-21 in the generation of inflammatory T cells. *Nature* **448**, 480–483 (2007).
24. Suto, A., Wurster, A.L., Reiner, S.L. & Grusby, M.J. IL-21 inhibits IFN-γ production in developing Th1 cells through the repression of Eomesodermin expression. *J. Immunol.* **177**, 3721–3727 (2006).
25. Yagi, R. *et al.* The transcription factor GATA3 actively represses RUNX3 protein-regulated production of interferon-γ. *Immunity* **32**, 507–517 (2010).
26. Awasthi, A. *et al.* Cutting edge: IL-23 receptor gfp reporter mice reveal distinct populations of IL-17-producing cells. *J. Immunol.* **182**, 5904–5908 (2009).
27. Chu, C.Q., Wittmer, S. & Dalton, D.K. Failure to suppress the expansion of the activated CD4 T cell population in interferon γ-deficient mice leads to exacerbation of experimental autoimmune encephalomyelitis. *J. Exp. Med.* **192**, 123–128 (2000).
28. Dubois, S., Mariner, J., Waldmann, T.A. & Tagaya, Y. IL-15Rα recycles and presents IL-15 In trans to neighboring cells. *Immunity* **17**, 537–547 (2002).
29. Plun-Favreau, H. *et al.* The ciliary neurotrophic factor receptor α component induces the secretion of and is required for functional responses to cardiotrophin-like cytokine. *EMBO J.* **20**, 1692–1703 (2001).
30. Wuest, S.C. *et al.* A role for interleukin-2 trans-presentation in dendritic cell-mediated T cell activation in humans, as revealed by daclizumab therapy. *Nat. Med.* **17**, 604–609 (2011).
31. Tussiwand, R. & Gautier, E.L. Transcriptional regulation of mononuclear phagocyte development. *Front. Immunol.* **6**, 533 (2015).
32. Lewis, K.L. *et al.* Notch2 receptor signaling controls functional differentiation of dendritic cells in the spleen and intestine. *Immunity* **35**, 780–791 (2011).
33. Croxford, A.L., Mair, F. & Becher, B. IL-23: one cytokine in control of autoimmunity. *Eur. J. Immunol.* **42**, 2263–2273 (2012).
34. Tanaka, T. *et al.* Enhancement of T helper2 response in the absence of interleukin (IL-)6; an inhibition of IL-4-mediated T helper2 cell differentiation by IL-6. *Cytokine* **13**, 193–201 (2001).
35. Diehl, S. & Rincón, M. The two faces of IL-6 on Th1/Th2 differentiation. *Mol. Immunol.* **39**, 531–536 (2002).

ONLINE METHODS

Generation of *Il6*RD mice. To generate a new conditional IL-6 reporter-depleter strain (*Il6*RD; *Il6*$^{tm3307(Cerulean–P2A–CD90.1)Arte}$) to allow the detection and specific depletion of IL-6 producing cells, we targeted exon 2 of the *Il6* locus on chromosome 5 by insertion of a *lox*P-flanked transcription-termination (stop) cassette followed by a reporter cassette. The reporter expression cassette comprised the following: the fluorescent reporter Cerulean, amplified by PCR from the cloning vector pDH51-GW-CFP; 2A peptide from *Porcine teschovirus-1* (P2A), the amino acid sequence GSGATNFSLLKQAGDVEENPGP[36] was synthetically attached to the adjacent sequences using oligonucleotides; Thy1.1 (CD90.1) surface protein that is in C57BL/6 mice (endogenously expressing alleles encoding Thy1.2 (CD90.2)) exclusively expressed on *Il6*-reporter-positive cells. The sequence was provided by M.S-S, and is identical to the GenBank accession code AAR17087.1; and the polyadenylation signal BGH pA, derived from the plasmid pcDNA3.1(+). A targeting vector MW21214 containing the *lox*P-flanked STOP cassette and the reporter-expression cassette was generated. To target this construct to the *Il6* locus, homologous arms were amplified from BAC clone C57BL/6J RPCIB-731. The SHA (short homologous arm) encompassed ~4 kb upstream of *Il6*, exon1, intron 1 and 31 nucleotides of exon 2. The natural exon 1 contains the 5′ untranslated region and the translation-initiation codon (START), which was mutated in the targeting vector (noSTART) by site-directed mutagenesis (from ATG to AAG) to prevent transcription of the remaining mouse *Il6* gene. Downstream of the expression cassette, a positive selection marker (CAGGS-promoter-driven puromycin resistance) was inserted, flanked by FRT sites, which allowed Flp-mediated deletion of the selection marker. The downstream LHA (long homologous arm) consisting of 5.7 kb of the *Il6* gene encompassed the remaining 153 nucleotides of exon 2, the complete intron 2, exon 3, intron 3, exon 4, and a partial intron 4. With the exception of the mutated start codon in exon 1, the genomic sequence was left intact to preserve all potential regulatory elements of *Il6*. For negative selection, a PGK-promoter-driven HSV TK was inserted. The targeting vector MW21214 was approved by complete sequencing, linearized by NotI and transfected into the C57BL/6N embryonic stem (ES) cell line Art B6 3.6 by electroporation to generate heterozygous targeted ES cells. Homologous recombinant clones were isolated using positive (PuroR) and negative (TK) selections. Clones were screened by PCR, resulting in 22% targeting frequency. The majority of the clones analyzed carried the inserted point mutation of the start codon. Four clones were expanded and validated by Southern blot and PCR analyses. Targeted ES cells were injected into blastocysts (isolated at 3.5 d after coitus from superovulated, mated BALB/c females). Injected blastocysts were transferred into pseudopregnant NMRI females (2.5 days after coitus). Chimerism was evaluated by coat color, and highly chimeric mice were bred to Flp-Deleter mice (C57BL/6-Tg$^{(CAG–Flpe)2Arte}$), which allowed the identification of germline transmission and Flp-mediated deletion of the positive selection marker. *Il6*RD mice were crossed with CMV-Cre (Tg(CMV-cre)^{1Cgn}) mice for ubiquitous expression or with CD11c-Cre (Tg(Itgax-cre)$^{1–1Reiz}$) mice for DC-specific, conditional expression of the reporter cassette after Cre-mediated removal of the STOP cassette. Under control of the endogenous *Il6* promoter, a chimeric transcript harboring the Cerulean open reading frame fused to the P2A sequence and the CD90.1 open reading frame is expressed. The P2A provides effective co-translational cleavage *in vitro* and *in vivo*, resulting in strict stoichiometric co-expression of individual Cerulean and CD90.1 proteins with correct subcellular localization (cytoplasm or cell surface, respectively).

Mice. *Il6*$^{flox/flox}$ (Il6$^{tm1.1Jho}$) mice[8,37], Foxp3.*gpf* KI (*Foxp3*^{tm1Kuch}) mice[5,36,38], Il23r.*gfp* KI (*Il23r*^{tm1Kuch}) mice[26] and 2D2 (Tg*(Tcra2D2,Tcrb2D2)*^{1Kuch}) mice[39] were described previously. *Il6*$^{-/-}$ (*Il6*^{tm1Kopf}) mice were obtained from Jackson Laboratory. *Il6ra*$^{flox/flox}$ mice were provided by T.F.W.[40]. OT-II mice (Tg*(TcraTcrb)*^{425Cbn}) with the congenic marker CD45.1 were provided by D. Busch (Institute for Medical Microbiology, Immunology and Hygiene, TU Munich). *Stat3*$^{flox/flox}$ (*Stat3*^{tm2Aki}) mice were from F. Greten (Institute for Tumor Biology and Experimental Therapy, Georg-Speyer Haus, Frankfurt). Mice with transgenic expression of sgp130-Fc were previously described[41]. For the EAE experiments reported in **Supplementary Figure 10**, opt_sgp130-Fc mice were used. To generate mice with cell-type-specific excision of *lox*P-flanked cassettes, mice with *lox*P-flanked alleles were bred with CD11c Cre (Tg(*Itgax-cre*)$^{1–1Reiz}$) mice, CD4 Cre (Tg(*Cd4-cre*)^{1Cwi}) mice, CD19 Cre (*Cd19*$^{tm1(cre)Cgn}$) mice or LysM Cre (*Lyz2*$^{tm1(cre)Ifo}$) mice (all from Jackson Laboratory). To visualize Cre-expressing cells, for some experiments, a Cre reporter allele Gt(ROSA)26Sor$^{tm1(EYFP)Cos}$ was crossed in (R26 STOP$^{flox/flox}$ YFP). All mouse strains were on pure C57BL/6 background. Animals were kept in a specific pathogen-free facility at the TU Munich or Johannes Gutenberg University Mainz. All experimental protocols were approved by the standing committee for experimentation with laboratory animals of the Bavarian or Rhine Palatinate state authorities and carried out in accordance with the corresponding guidelines (AZ 55.2-1-54-2532-29-13, AZ 55.2-1-54-2532-95-14 and 23 177-07/G 13-1-099).

Induction of EAE. To induce EAE, mice were immunized subcutaneously (base of tail) with 200 µl of an emulsion containing 200 µg MOG(35–55) (MEVGWYRSPFSRVVHLYRNGK; Auspep, Tullamarine, Australia) and 500 µg *Mycobacterium tuberculosis* H37Ra (BD Difco) in CFA and received 200 ng pertussis toxin (PTx,Sigma) intravenously on the day of and 2 d after the immunization. Clinical signs of disease were monitored as described previously[42]. To ablate *Il6*-reporter- (Thy1.1)-expressing cells, mice were treated with intraperitoneal injections of anti-Thy1.1 (19E12) or isotype-matched control antibody (mouse IgG2a; C1.18.4). For *in vivo* neutralization of IFN-γ, mice received anti-IFN-γ (R4-6A2) or isotype-matched control antibody (rat IgG1; HRPN). Antibodies were obtained from BioXCell and were injected at a dose of 200 µg starting 1 d after immunization, followed by injections every other day until the development of first signs of disease. For adoptive-transfer experiments, recipient mice received 2.5×10^6 naive GFP$^-$ (Foxp3$^-$) 2D2 cells intravenously 1 d before immunization.

Preparation of CNS mononuclear cells. At the peak of disease, CNS-infiltrating cells were isolated after perfusion through the left cardiac ventricle with PBS. Brain and spinal cord were dissected and digested with collagenase D (2.5 mg/ml) and DNase I (1 mg/ml) at 37 °C for 45 min. After passing the tissue through a 70-µm cell strainer, cells were separated by discontinuous Percoll gradient (70%/37%) centrifugation. Mononuclear cells were isolated from the interphase.

Preparation of naive T cells and differentiation of helper T cell subsets. Naive helper T cells were isolated from peripheral lymph nodes and spleens. Naive T cells were isolated using magnetic beads (Naive CD4$^+$ T Cell Isolation Kit, Miltenyi Biotec) or subsequent to enrichment of helper T cells (CD4$^+$ T Cell Isolation Kit, untouched, Miltenyi Biotec) by flow cytometry (CD4$^+$CD44^{low} GFP$^-$ (Foxp3$^-$)). For helper T cell differentiation, naive T cells were stimulated for 3 d with plate-bound antibody to CD3 (145-2C11, 4 µg/ml, BioXCell) and soluble antibody to CD28 (PV-1, 2 µg/ml, BioXCell). Recombinant cytokines were added to the differentiation cultures: human TGF-β1 (0.25 to 2 ng/ml) and/or mouse IL-6 (50 ng/ml), all R&D Systems. In some experiments, we compared soluble human IL-6 (Miltenyi) with hyper-IL-6 (ref. 19) in equimolar amounts (ranging from 0.013 nM to 1.3 nM) in the presence of TGF-β (0.1–0.5 ng/ml). Cells were cultured in Dulbecco's modified Eagle medium (DMEM) supplemented with 10% FCS, 50 µM β-mercaptoethanol, nonessential amino acids (MEM-NEAA), MEM vitamins, folic acid, 50 U/ml penicillin, 50 µg/ml streptomycin and 0.1 mg/ml gentamicin.

Isolation of DCs. Peripheral lymph nodes and spleens were injected with digestion mix (1 mg/ml collagenase D and 20 µg/ml DNase I (Roche), 2% FCS in HEPES-buffered RPMI-1640). Organs were fragmented and incubated at 37 °C for 45 min. To disrupt cell complexes, 10 mM EDTA was added for additional 5 min. Cell suspensions were passed through 100-µm cell strainers.

Generation and culture of BMDCs. BMDCs were generated by flushing out femora and tibiae. Viable cells were cultured in clone medium supplemented with GM-CSF and IL-4 (both 20 ng/ml, R&D Systems) for 6 d with splitting every other day. DCs were removed by vigorous pipetting and cultured in the presence of TLR ligands CpG (ODN 1826) from InVivoGen or LPS (*E.coli* 0111:B4 Lipopolysaccharide), Sigma-Aldrich.

BMDC–T cell co-culture. Naive 2D2 T cells were pre-cultured overnight (at a ratio of 1:4) with splenocytes or BMDCs from *Il6*$^{flox/flox}$ mice, *Il6*$^{-/-}$ mice or

doi:10.1038/ni.3632

Il6$^{\Delta DC}$ mice in the presence of 50 μg/ml MOG(35–55). For some experiments, naive 2D2 and OT-II T cells were pre-cultured with BMDCs in the presence of either MOG(35–55) or OVA(323–339) (ISQAVHAAHAEINEAGR; Auspep, Tullamarine, Australia). LPS (0.5 μg/ml) was added, and cells were harvested at the time points for analysis indicated in the figures and legends. In some experiments, the matrix-metalloproteinase inhibitor Marimastat (3 μM, Sigma-Aldrich) was added to block IL-6Rα shedding. To analyze different IL-6 signaling modes, blocking agents were added: anti-IL6 (polyclonal goat IgG, R&D # AF-406-NA or monoclonal mAb#8 (ref. 43)), anti-IL6Rα (MR16-1), or sgp130-Fc[14], all at 1 μg/ml.

Flow cytometry and intracellular cytokine staining. Cells were stained with live/dead fixable dyes (Aqua (405 nm exc) or Near-IR (633 nm exc), Invitrogen) and antibodies (1:100 dilution unless specified otherwise) to the following surface markers: CD4 (GK1.5 or RM4-5), CD11b (M1/70), CD11c (HL3), CD44 (IM7; 1:400), CD69 (H1.2F3), TCRVβ8.1/2 (MR5-2), TCRVβ8.3 (1B3.3), 2D2 TCR Vα3.2 (RR3-16) or Vβ11 (RR3-15; all from BD Biosciences); CD19 (6D5; 1:200), CD45.2 (104; 1:200), Thy1.1 (CD90.1, Ox-7), CD96 (3.3), CD126 (IL-6Rα, D7715A7), CD172 (SIRPα, P84), Ly6G (1A8; 1:200) or NK1.1 (PK136; all from BioLegend); and CD3 (clone 145-2C11), CD25 (PC61; 1:200), CD45.1 (A20; 1:400), CD103 (2E7), CD130 (gp130, KGP130), major histocompatibility complex class II (M5/114.15.2; 1:200), SiglecH (eBio440c; all from eBioscience). Nonspecific antibody binding was blocked by Fc Block (anti CD16/CD32; 1:100; BD Biosciences).

For intracellular cytokine staining, cells were re-stimulated with 50 ng/ml PMA (Sigma-Aldrich), 1 μg/ml ionomycin (Sigma-Aldrich) and monensin (1 μl/ml BD GolgiStop) at 37 °C for 2.5 h. Subsequent to live/dead and surface staining, cells were fixed and permeabilized (Cytofix/Cytoperm and Perm/Wash Buffer; BD Biosciences), and stained for cytokines IL-17A (TC11-18H10.1; 1:100; BioLegend), IFN-γ (XMG1.2; 1:200; eBioscience), IL-10 (JES5-16E3; 1:100; BD Biosciences), and GM-CSF (MP1-22E9; 1:100;, BD Biosciences). For intracellular staining of IL-6 in BMDCs, cells were stimulated with TLR ligands for 3 h before adding 5 μg/ml Brefeldin A (Sigma-Aldrich) for further 2 h. Subsequent to live/dead and surface staining, fixation and permeabilization, cells were stained for IL-6 (MP5-20F3; 1:100; BD Biosciences). For intranuclear staining of Foxp3 (FJK-16s, eBioscience; 1:100), cells were stained for live/dead discrimination and surface markers. Fixation, permeabilization, and intranuclear staining were performed according to the manufacturer's instructions (Transcription Factor Staining Buffer Set, eBioscience). To analyze STAT3 activation, cells were fixed with Phosflow Lyse/Fix Buffer (BD) for 10 min at 37 °C, permeabilized with PhosFlow Perm Buffer III (BD) for 30 min on ice and stained simultaneously for surface markers and STAT3 phosphorylated at Tyr705 (4/P-STAT3; 1:20; BD Biosciences) according to the manufacturer's instructions. Cells were analyzed using a CyAn ADP 9 flow cytometer (Beckman/Coulter) and FlowJo software (Tree Star).

Detection of antigen-specific T cells *ex vivo*. MOG-specific cytokine producing helper T cells were analyzed around days 7–8 after immunization. Single-cell suspensions from draining lymph nodes or spleens were restimulated with 30 μg/ml MOG(35–55) for 6 h in the presence of 5 μg/ml brefeldin A during the last 3 h of incubation, followed by surface and intracellular cytokine staining as described above. MOG-specific T cells were detected via staining of fixed and permeabilized cells with biotinylated anti-CD40L (CD154, clone MR1; 1:100; eBioscience) and fluorochrome-coupled streptavidin.

ELISA. IL-6 amounts in cell culture supernatant and in the serum of immunized mice were quantified using standard sandwich ELISA (R&D Systems, DuoSet). Standard curves and sample concentrations were calculated based on the mean of triplicates for each dilution or sample.

Quantitative PCR analysis. For quantitative PCR, RNA was extracted using RNeasy columns (Qiagen). cDNA was transcribed using TaqMan Reverse Transcription Reagents as recommended (Applied Biosystems) and used as template for quantitative PCR. Primer plus FAM-labeled probe mixtures were obtained from Applied Biosystems (*Il1b*: Mm00434228_m1; *Il6*: Mm99999064_m1; *Il12a* (*p35*): Mm00434165_m1; *Il12b* (*p40*): Mm01288989_m1; *Il23a* (*p19*): Mm00518984_m1; *Eomes*: Mm01351985_m1; *Rorc*: Mm00441144_g1; *Tbx21*: Mm00450960_m1). The gene expression was normalized to the expression of the gene encoding β-actin (ACTB, VIC-labeled probe).

RNA sequencing. Total RNA was isolated from 2D2 GFP$^-$ (Foxp3$^-$) T cells sorted by flow cytometry and re-isolated from draining lymph nodes after priming in *Il6*$^{flox/flox}$ host mice, *Il6*$^{-/-}$ host mice or *Il6*$^{\Delta DC}$ host mice. Total RNA was further purified with AmpureXP beads to remove impurities detected by UVvis spectrometry. This RNA was used to construct sequencing libraries using the Encore Complete RNA-Seq library system (NuGen Inc. Santa Clara, USA) according to the instructions of the manufacturer. In brief, 125 ng of total RNA were treated with heat-labile ds DNAse (Thermo Scientific Inc., MA, USA) to remove residual DNA and used for mixed random- or poly(A)-primed first-strand cDNA synthesis. After second-strand synthesis, the double-stranded cDNA was fragmented by sonication (Covaris M220; power 50 W, duty factor 20, 200 cycles per burst, 115 s treatment time). The fragmented cDNA was end repaired and ligated with sample-specific barcoded adaptors. After strand selection, the library was amplified (four cycles of 94 °C for 30 s, 55 °C for 30 s and 72 °C for 60 s and 12 cycles of 94 °C for 30 s, 63 °C for 30 s and 72 °C for 60 s) and purified and size-selected with AMPure XP beads (Beckman Coulter, CA, USA). Resulting libraries were quantified on a Bioanalyzer 2100 (Agilent, Santa Clara, USA). The barcoded libraries were pooled at 10 nM concentration for multiplexed sequencing. All libraries were sequenced on a HiSeq 1500 as 100-base single reads to a depth of 25–30 Mio raw reads per sample. After demultiplexing of sequence data, adaptor sequences and poly(A) tails were removed and each library was mapped to the murine reference genome mm10 with the spliced-read aligner STAR[44]. Based on the mapping results, sequence reads for annotated genes were counted with HTSeq[45]. Comparative analyses of gene expression were performed with the DEseq2 package[46] as pairwise comparison of two groups for each combination of interest. The false-discovery rate for detection of differentially abundant transcripts was set to 5%.

For gene-set–enrichment analysis (GSEA), a ranked list of the change (fold values) in RNA-sequencing read values or nanostring signals between *Il6*$^{flox/flox}$ primed and *Il6*$^{\Delta DC}$ primed effector T cells isolated from draining lymph nodes was calculated. The java GSEA Desktop Application v2.2.1 was used in conjunction with the Molecular Signatures Database v45.1 to run the analysis. Data analysis of genes enriched differentially in wild type-primed and *Il6*$^{\Delta DC}$ primed Foxp3$^-$ 2D2 T cells was performed through the use of QIAGEN's Ingenuity Pathway Analysis (IPA, QIAGEN Redwood City, http://www.qiagen.com/ingenuity). The Molecule Activity Predictor (MAP) tool was used to investigate the effect of IL-6 signaling pathways on identified IL-6 target genes.

Immunofluorescence, PLA and confocal microscopy. Naive 2D2 T cells were cultured at a ratio of approximately 4:1 with BMDCs labeled with CellTracker Deep Red (Molecular Probes) in chamber slides in the presence of MOG(35–55) to form immunological synapses. Subsequent to LPS stimulation for 80 min, cells were fixed with ice-cold methanol, blocked and permeabilized in PBS containing 10% normal goat serum, 1% BSA and 0.2% Triton X-100. Incubation with primary antibody specific for IL-6 (polyclonal goat IgG, R&D # AF-406-NA) diluted at 12.5 μg/ml in PBS supplemented with 1% BSA and 0.1% Tween 20 was carried out overnight at room temperature. Secondary antibody (chicken anti-goat IgG_AF 488 conjugate; Invitrogen) was diluted 1:1,000 in PBS supplemented with 1% BSA and 0.1% Tween 20 and incubated for 1 h at room temperature. Samples were mounted with ProLong Gold Antifade Reagent with DAPI (Molecular Probes) for nuclear counterstaining.

To visualize IL-6–IL-6Rα complexes, PLA was performed according to the manufacturer's instructions (Duolink *In situ* Red Kit Goat/Rabbit, Sigma-Aldrich) using primary antibodies specific for IL-6 (polyclonal goat IgG; R&D # AF-406-NA; 12.5 μg/ml) and IL-6Rα (polyclonal rabbit IgG M-20, Santa Cruz #660; 4 μg/ml).

Confocal image stacks were recorded on a confocal microscope (Olympus FV1000) equipped with ×60/1.42 N.A. oil-immersion objective. All images were acquired sequentially. Maximum intensity projections and *xz* representations were generated using the open-source image-analysis software Fiji[47]. Gamma was adjusted nonlinearly to enhance visibility of morphological details.

Statistical analysis. Statistical evaluations of cell frequency measurements, cell numbers, mRNA amounts and protein levels were performed with the

unpaired Student's *t*-test when two populations were compared. Two-tailed *P* values < 0.05 were considered significant. Multiple comparisons were performed with one-way ANOVA followed by post-hoc multiple comparisons tests as indicated in the legends to the figures. Comparison of EAE scores in groups (analyzed as disease burden per individual day) was done with one-way-ANOVA and post-hoc test as indicated in the legends to the figures.

Data-availability statement. Supporting data are available from T.K. (thomas.korn@tum.de).

36. Kim, J.H. *et al.* High cleavage efficiency of a 2A peptide derived from porcine teschovirus-1 in human cell lines, zebrafish and mice. *PLoS One* **6**, e18556 (2011).
37. Quintana, A. *et al.* Astrocyte-specific deficiency of interleukin-6 and its receptor reveal specific roles in survival, body weight and behavior. *Brain Behav. Immun.* **27**, 162–173 (2013).
38. Korn, T. *et al.* Myelin-specific regulatory T cells accumulate in the CNS but fail to control autoimmune inflammation. *Nat. Med.* **13**, 423–431 (2007).
39. Bettelli, E. *et al.* Myelin oligodendrocyte glycoprotein-specific T cell receptor transgenic mice develop spontaneous autoimmune optic neuritis. *J. Exp. Med.* **197**, 1073–1081 (2003).
40. Wunderlich, F.T. *et al.* Interleukin-6 signaling in liver-parenchymal cells suppresses hepatic inflammation and improves systemic insulin action. *Cell Metab.* **12**, 237–249 (2010).
41. Rabe, B. *et al.* Transgenic blockade of interleukin 6 transsignaling abrogates inflammation. *Blood* **111**, 1021–1028 (2008).
42. Korn, T. *et al.* IL-6 controls Th17 immunity in vivo by inhibiting the conversion of conventional T cells into Foxp3+ regulatory T cells. *Proc. Natl. Acad. Sci. USA* **105**, 18460–18465 (2008).
43. Brakenhoff, J.P., Hart, M., De Groot, E.R., Di Padova, F. & Aarden, L.A. Structure-function analysis of human IL-6. Epitope mapping of neutralizing monoclonal antibodies with amino- and carboxyl-terminal deletion mutants. *J. Immunol.* **145**, 561–568 (1990).
44. Dobin, A. *et al.* STAR: ultrafast universal RNA-seq aligner. *Bioinformatics* **29**, 15–21 (2013).
45. Anders, S., Pyl, P.T. & Huber, W. HTSeq--a Python framework to work with high-throughput sequencing data. *Bioinformatics* **31**, 166–169 (2015).
46. Love, M.I., Huber, W. & Anders, S. Moderated estimation of fold change and dispersion for RNA-seq data with DESeq2. *Genome Biol.* **15**, 550 (2014).
47. Schindelin, J. *et al.* Fiji: an open-source platform for biological-image analysis. *Nat. Methods* **9**, 676–682 (2012).

doi:10.1038/ni.3632

Corrigendum: Trans-presentation of IL-6 by dendritic cells is required for the priming of pathogenic T_H17 cells

Sylvia Heink, Nir Yogev, Christoph Garbers, Marina Herwerth, Lilian Aly, Christiane Gasperi, Veronika Husterer, Andrew L Croxford, Katja Möller-Hackbarth, Harald S Bartsch, Karl Sotlar, Stefan Krebs, Tommy Regen, Helmut Blum, Bernhard Hemmer, Thomas Misgeld, Thomas F Wunderlich, Juan Hidalgo, Mohamed Oukka, Stefan Rose-John, Marc Schmidt-Supprian, Ari Waisman & Thomas Korn
***Nat. Immunol.* 18, 74-85 (2017); published online 28 November 2016; corrected after print 23 January 2017**

In the version of this article initially published, the label for third bar from the left in Figure 4f ('Anti-IL-6α') was incorrect; the correct label is 'Anti-IL-6Rα'. Also, in the legend for Figure 4f, the description of the treatment conditions for middle four bars ('medium alone, or LPS and anti-IL-6 (MR16-1 or polyclonal antibody), anti-IL-6R (mAb#8)') was incorrect; the correct description is 'LPS alone (Medium), or LPS and anti-IL-6Rα (MR16-1), anti-IL-6 (polyclonal antibody or mAb#8)'. The error has been corrected for the print, PDF and HTML versions of this article.